Geomorphology 414 (2022) 108363

Contents lists available at ScienceDirect

Geomorphology

journal homepage: www.journals.elsevier.com/geomorphology

Influence of rheology on landslide-dammed lake impoundment and sediment trapping: Back-analysis of the Hintersee landslide dam

Anne-Laure Argentin [a,*,1], Thomas Hauthaler [a,1], Moritz Liebl [a], Jörg Robl [a], Stefan Hergarten [b], Günther Prasicek [a,c], Bernhard Salcher [a], Daniel Hölbling [d], Claire Pfalzner-Gibbon [e], Lisa Mandl [e,f], Michael Maroschek [e,f], Lorena Abad [d], Zahra Dabiri [d]

[a] Department of Geography and Geology, University of Salzburg, 5020 Salzburg, Austria
[b] Near Surface Geophysics, Institute of Earth and Environmental Sciences, Faculty of Environment and Natural Resources, 79104 Freiburg, Germany
[c] Centre for Interdisciplinary Mountain Research, University of Lausanne, 1967 Bramois, Switzerland
[d] Department of Geoinformatics - ZGIS, University of Salzburg, 5020 Salzburg, Austria
[e] Berchtesgaden National Park, 83471 Berchtesgaden, Germany
[f] Ecosystem Dynamics and Forest Management Group, Technical University of Munich, 85354 Freising, Germany

ARTICLE INFO

Keywords:
Landslide dam
Landslide-dammed lake
Landslide
Landscape evolution
Erosion
Sediment storage

ABSTRACT

Lacustrine deltas that develop upstream of landslide-dammed lakes can trap and store fluvial sediments. The development of these deltas and their size are conditioned by the geometry of the dam, which is in turn influenced by the landslide rheology. In this study, we back-analyze the formation of the Hintersee landslide-dammed lake in southeastern Germany and investigate the impact of landslide rheology on lake volume and sediment trapping capacity. We use the Voellmy rheology, a rheological model defined by two parameters, μ and ξ, and find that landslide rheology strongly influences sediment trapping. The Voellmy dry friction μ shows a non-linear relationship with lake volume and sediment trapping, while the velocity squared drag ξ has less impact. The Hintersee landslide dam presents a sediment trapping capacity of up to three times the volume of the landslide-dammed lake. Thus, the impact of landslide dams on sediment transport is underestimated by up to a factor of 3 when using lake volume as a proxy for sediment trapping capacity. We find that friction exhibits a non-linear relationship with lake volume and sediment trapping, while velocity has a more limited influence.

1. Introduction

Landslide dams form when a landslide buries a riverbed, blocking the river flow, creating a lake, and potentially trapping sediments. These dams pose a high risk of flooding to settlements and infrastructure: upstream because they impound water, and downstream because they are highly unstable. Indeed, more than half of them fail within the first ten days of their formation (Costa and Schuster, 1988). However, some landslide dams last for thousands of years and act as considerable sediment traps (Fan et al., 2012) before they are incised by fluvial erosion (e.g., Savelli et al., 2013). According to Fan et al. (2012), a high proportion of sediment from earthquake-triggered landslides ends up trapped in landslide-dammed lakes (e.g., 14 to 18% for the 2008 Wenchuan earthquake). This pattern can also be observed in the Himalayas, where Blöthe and Korup (2013) estimate that 44% of mountain sediments, including mass-wasting deposits, are trapped as valley fills. The sediments form a lacustrine delta behind the dam, with the delta plain surface following a characteristic slope angle (Ouimet et al., 2007), which can be directly measured on the local longitudinal stream profile. The value taken by this angle depends on the location of the dam within the mountain range and tends to decrease with increasing stream order and mean elevation. We define trapping capacity as the maximum volume of sediment that can be stored in the sediment trap.

Landslide dams influence watershed evolution by impacting sediment supply to streams and forming new local base levels and knickpoints (Ouimet et al., 2007). By creating lakes and trapping sediments, landslide dams reduce the sediment load of the river downstream: after the Wenchuan earthquake (Fan et al., 2012), sediment supply to rivers was delayed from weeks to years.

With the remobilization of accumulated sediments, the sediment

* Corresponding author.
E-mail address: anne-laure.argentin@plus.ac.at (A.-L. Argentin).
[1] These authors contributed equally to this work

https://doi.org/10.1016/j.geomorph.2022.108363
Received 26 January 2022; Received in revised form 26 June 2022; Accepted 27 June 2022
Available online 7 July 2022

load and incision rates of the river are again altered. Landslide dams induce spatial variations in fluvial incision rates (Korup, 2005): they can act as local base levels, inducing lower river gradients upstream of their location, preserving the upstream topography from incision. By forming sediment traps, landslide dams act as buffers to erosion and protect upstream landscapes, contributing to the formation of relict landscapes. Sediment traps can be studied by conducting a sediment budget assessment (Cossart and Fort, 2008; Hinderer, 2012, 2001). Common practice relies on the mapping of the deposits (Cossart and Fort, 2008) to infer the geometry of the sediment compartment, although modeling is also possible (e.g., with Petrel®, Pomper et al., 2017; Wang et al., 2014). Sediment budget assessments have already been applied to several infilled landslide dams. For example, Cossart and Fort (2008) reconstructed the pre-landslide topography of two landslide dams in the French Southern Alps and showed that landslide dams exert a sustained control on sediment fluxes. The sediment trap capacity of landslide dams is important for understanding the impact of these events on the landscape.

From these sediment budget assessments, the millennial erosion rates in the European Alps can be constrained (Hinderer, 2001). They vary spatially and temporally: the Western Alps tend to present slightly higher millennial erosion rates than the Eastern Alps, while the highest

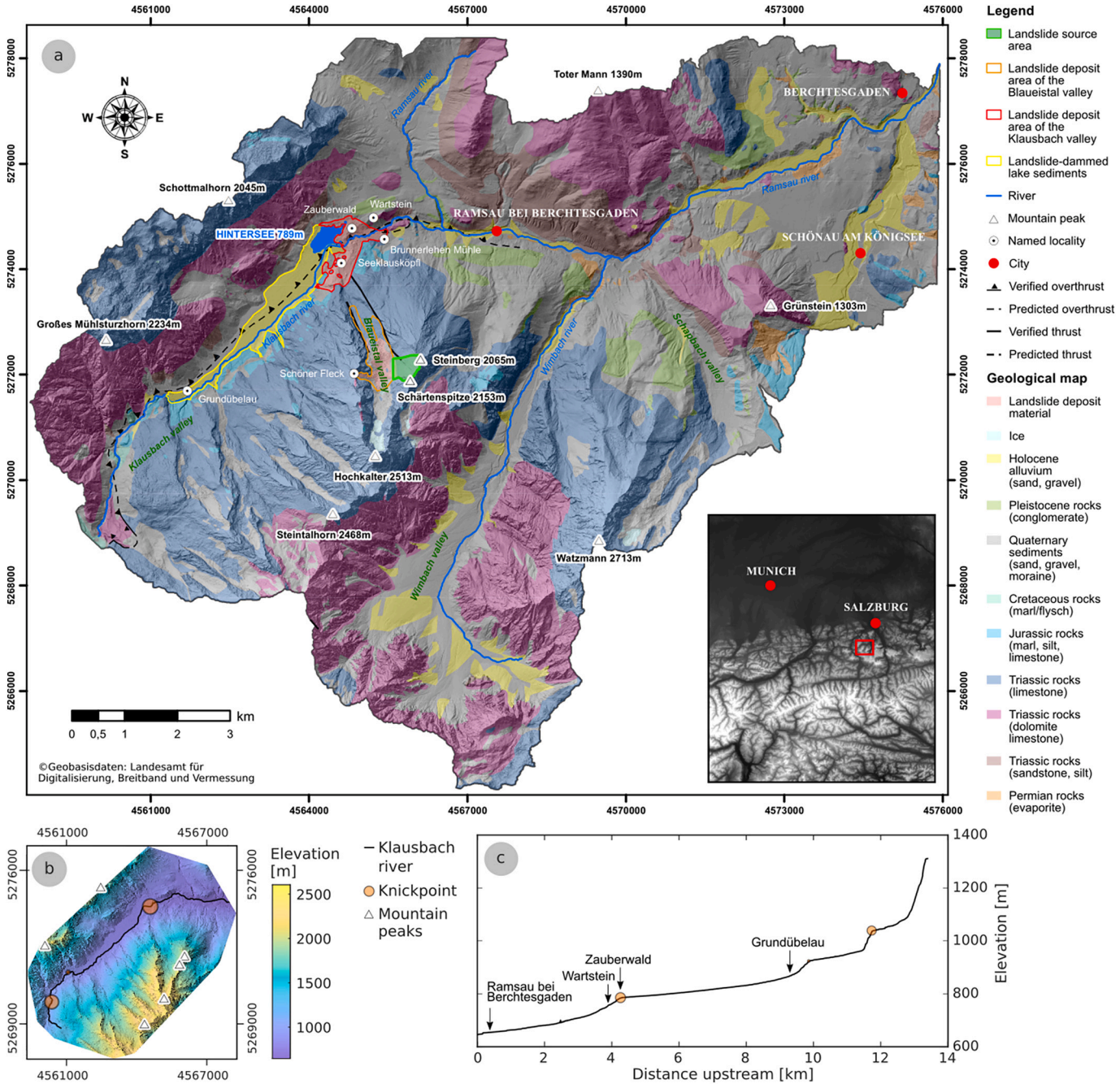

Fig. 1. a) Geological map of the Hintersee landslide-dammed lake, which formed 3591 ± 85 years ago on the Klausbach river, upstream of the Ramsauer Ache river, in the Bavarian Alps in southeastern Germany (von Poschinger and Thom, 1995), b) location of knickpoints along the Klausbach river (black line) and c) along the longitudinal profile of the Klausbach river. The landslide source area as described by von Poschinger and Thom (1995) is outlined in green, the Blaueistal valley (in German Blaueistal) landslide deposition area in orange, the Klausbach valley landslide deposition area in red, and the lake sediments in yellow. The Hintersee dam forms a knickpoint about 30 m high. We used the DHDN / Gauss-Krüger Zone 4 (EPSG:31468) projection system.

denudation rates (several millimeters per year) are reported for the Central Alps (Delunel et al., 2020; Codilean et al., 2018; Grischott et al., 2017; Glotzbach et al., 2013). Erosion rates can also vary considerably with rock type (e.g., Korup and Schlunegger, 2009).

The sediment trap capacity of a landslide-dam depends on the landslide rheology. Argentin et al. (2021) have shown that the landslide-dammed lake volume, and thus the sediment trap volume, is directly related to the landslide damming efficiency. The formation of a landslide dam depends on two factors: the local topography and the deposit shape. Indeed, landslide rheology impacts the formation of landslide dams (Hungr, 2011), but in a manner subject to local topography (Argentin et al., 2021). However, little is known about the influence of landslide rheology on the formation and capacity of sediment traps.

The aim of this study is to analyze the impact of landslide rheology on the volume and sediment trapping capacity of landslide-dammed lakes, using the Hintersee landslide-dammed lake at the boundary of the Berchtesgaden National Park in Bavaria, southeastern Germany, as a case study. We reconstruct the topography prior to landslide deposition and simulate the landslide that impounded the valley with a range of rheologies. We then calculate the lake and trapped sediment volumes.

1.1. The Hintersee study area

The Hintersee landslide-dammed lake is located at the beginning of the Klausbach valley in the Bavarian Alps, Germany, on the course of the Klausbach river, upstream of the Ramsauer Ache river (Fig. 1). The landslide dam was dated by the Geological Survey in Hannover to 3520 ± 85 years before present (von Poschinger and Thom, 1995, uncal.; calibrated ages are similar), and was thus formed between 1485 and 1655 BCE by a landslide originating from the eastern valley flank of the Schärtenspitze mountain (Bayerisches Geologisches Landesamt, 2005). The lithology consists predominantly of calcareous rock, mainly limestone to the south and dolomite to the north of the lake.

The landslide source area (green outline, Fig. 1a) is located on the Schärtenspitze mountain (Fig. 2a), on a cataclinal valley flank (von Poschinger and Thom, 1995), facilitating detachment. The original release volume is difficult to estimate from the topography, as the vegetation has recovered and the topography allows for several plausible scenarios. The rupture surface is assumed to extend from the Blaueistal valley floor to the top of the ridge, with a length varying from 300 to 500 m from east to west (Fig. 2b). According to von Poschinger and Thom (1995), although the northern boundary is left undetermined, the width of the rupture area is estimated to be 400 m while the average thickness varies between 70 and 100 m. Thus, the original release volume is evaluated to range between 12×10^6 m^3 and 16×10^6 m^3.

After detachment from the Schärtenspitze mountain, the landslide collided with the opposite flank of the Blaueistal valley, the Schöner Fleck, before continuing its trajectory toward the Klausbach valley (Fig. 2a). Von Poschinger and Thom (1995) appraised the maximum velocities reached by the Hintersee landslide at $45 - 60$ m.s^{-1}. By crashing into the Schöner Fleck flank, the landslide lost some velocity and partially settled in the Blaueistal valley (orange contour, Fig. 1a). The rest of the mass flowed down the valley into the Klausbach valley, blocking the river and forming a dam (red outline, Fig. 1a). Von Poschinger and Thom (1995) estimate the release volume at $12 - 16 \times 10^6$ m^3, the deposit volume in the Blaueistal valley at $0.5 - 3 \times 10^6$ m^3 and the deposit volume in the Klausbach valley at $15 - 18 \times 10^6$ m^3. They explain the volume increase by a factor of about 1.3 with bulking - the process by which the landslide scours the topography during runout and incorporates the eroded material into the moving mass (e.g., Scott et al., 2001). This bulking estimate is consistent with the average volume increase found by Hungr and Evans (2004) of up to 25% of the release volume. The area covered by deposits in the Klausbach valley is estimated to be $0.6 - 0.7$ km^2, and the deposits to be about 40 m thick.

The landslide dam, which blocked a 44 km^2 catchment, was eroded after its creation and is deemed to have failed once (von Poschinger and Thom, 1995). Indeed, several boulders of about 4 m can still be found downstream of the dam site (Fig. 2d, e), up to the South of the Wartstein in the Brunnerlehen Mühle, indicating a possible former catastrophic failure of the dam (von Poschinger and Thom, 1995). The present dam has been incised by the river, which has removed sediments in the downstream part and now flows through it (Fig. 2c).

The landslide dam formed a lake that extended much farther upstream than the present Hintersee (Fig. 2f). According to the interpretation of von Poschinger and Thom (1995), the landslide-dammed lake (yellow outline, Fig. 1a) may have extended as far as the Grundübelau, about 4 km upstream, which represents the last flat valley area before the more incised upstream valley. The dammed lake still exists today, although its surface area is deemed to have shrunk since its formation, due to sediment infilling by the Klausbach (Penck and Richter, 1885). In 1885, Penck and Richter (1885) estimated that 2000 m^2 of the lake's area was lost to sediment infilling over a three-year period. Over the past few centuries, several construction projects have been carried out upstream of the lake and on the dam to preserve the water impoundment and keep the lake from being completely infilled with sediments (von Poschinger and Thom, 1995).

2. Materials

We base our study on geologic maps, topographic data, subsurface modeling software, and previous field studies of von Poschinger and Thom (1995), which includes a geophysical longitudinal cross-section and two boreholes (Fig. 3, yellow). The geological map was derived from the Geological map of Berchtesgaden at 1:25.000 (Bayerisches Landesamt für Umwelt, 1993). The Berchtesgaden National Park provided us with a 1 m Digital Elevation Model (DEM) (Landesamt für Digitalisierung, 2017), acquired by full-waveform airborne laser scanning (LiDAR) in 2017. For computational reasons, we resampled the DEM to a lower resolution of 5 m, and then used the subsurface modeling software from the petroleum industry Petrel® to process it. The geophysical profile, obtained by seismic refraction and geoelectric depth sounding, was acquired by GEORISK (Bader, 1981; Risch, 1993). The profile covers approximately the length of the valley upstream of the dam and sets at 50 m the bottom of the landslide-dammed sediment layer. Boreholes KB 1 and KB 2 are 37 m and 20 m deep, respectively (Risch, 1993), and were drilled by the Bavarian Geological Survey for the GEORISK project (von Poschinger and Thom, 1995). None of the cores reach the bottom of the landslide-dammed lake sediments and the boreholes thus provide only a minimum depth constraint without indicating its precise measurement.

3. Methods

We recreate the formation of the landslide-dammed lake and its sediment trap in four steps (Fig. 3). (1) We reconstruct the topography of the valley and mountain flank before the landslide using ArcGIS (Desktop version 10.7.1) and Petrel® (2019). (2) We then simulate the landslide runout with Gerris (using 2D libgfs version 1.3.2). (3) We fill the resulting topography using GRASS GIS (version 7.6.2; Module r.terraflow) to create the lake. (4) We finally reconstruct the sedimented topography of the lake using the open source GIS application SAGA (Wang and Liu, 2006). All maps are plotted with GMT (Wessel et al., 2019), using the DHDN / Gauss-Krüger Zone 4 (EPSG:31468) projection system.

3.1. Reconstruction of the topography

To geometrically reconstruct part of the topography (Fig. 3, green), we combine selected elevation data points with the DEM contour lines. First, we define the extent of the DEM to be reconstructed and create a polyline with ArcGIS. Then, we extract the contour lines from the DEM and cut them with the extent polyline. We keep the parts outside the area

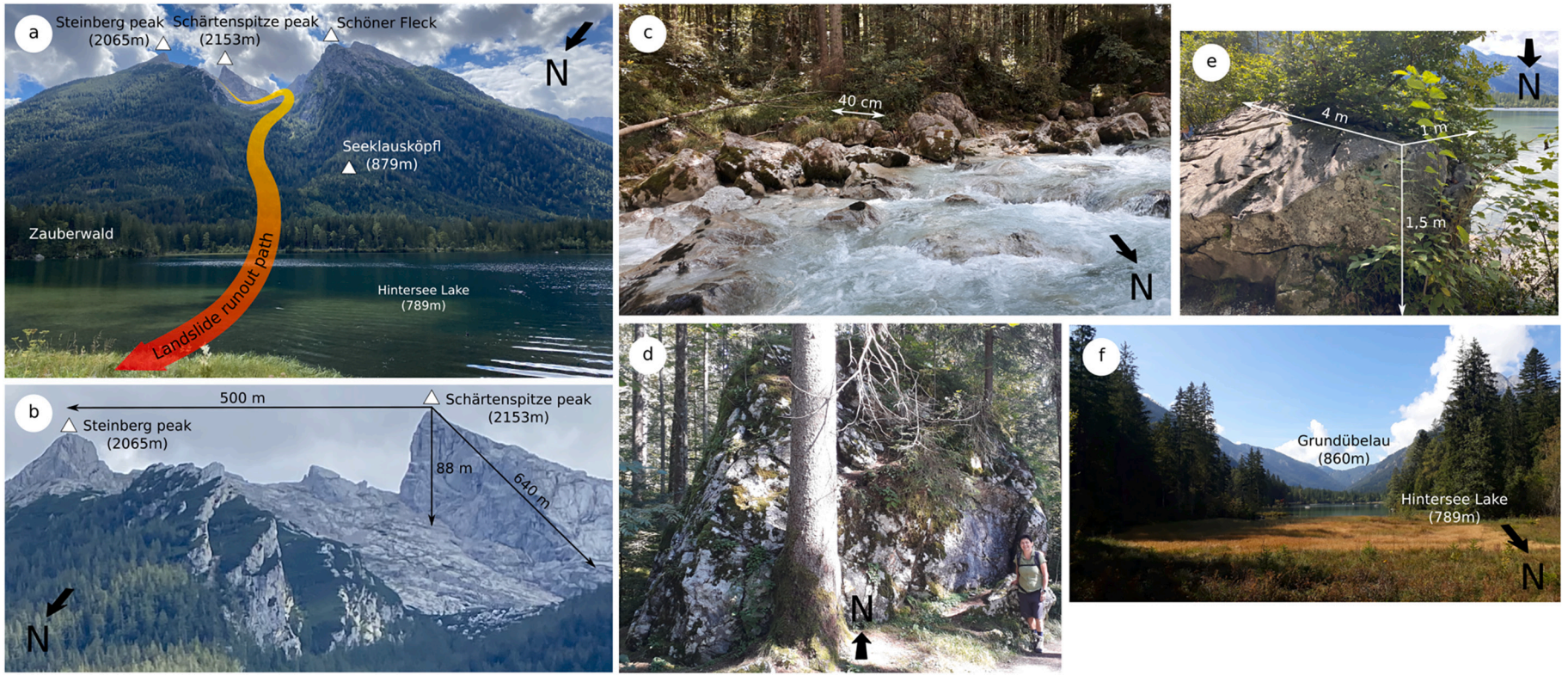

Fig. 2. a) Global view taken from the Western shore of the Hintersee lake, showing the runout path of the Hintersee landslide from the Schärtenspitze through the Blaueistal valley to the Zauberwald deposition area. The lake outlet is located behind the Zauberwald. b) Close-up view of the landslide source area, located between the Schärtenspitze and the Steinberg peak. c) Shores of the Klausbach river in the Zauberwald. The pebbles show no imbrication pattern and are angular. d) One of the biggest boulders that can be found in the Zauberwald. e) One of the many smaller boulders around the Hintersee lake. f) View in direction of the Hintersee lake and the upstream area of Grundübelau.

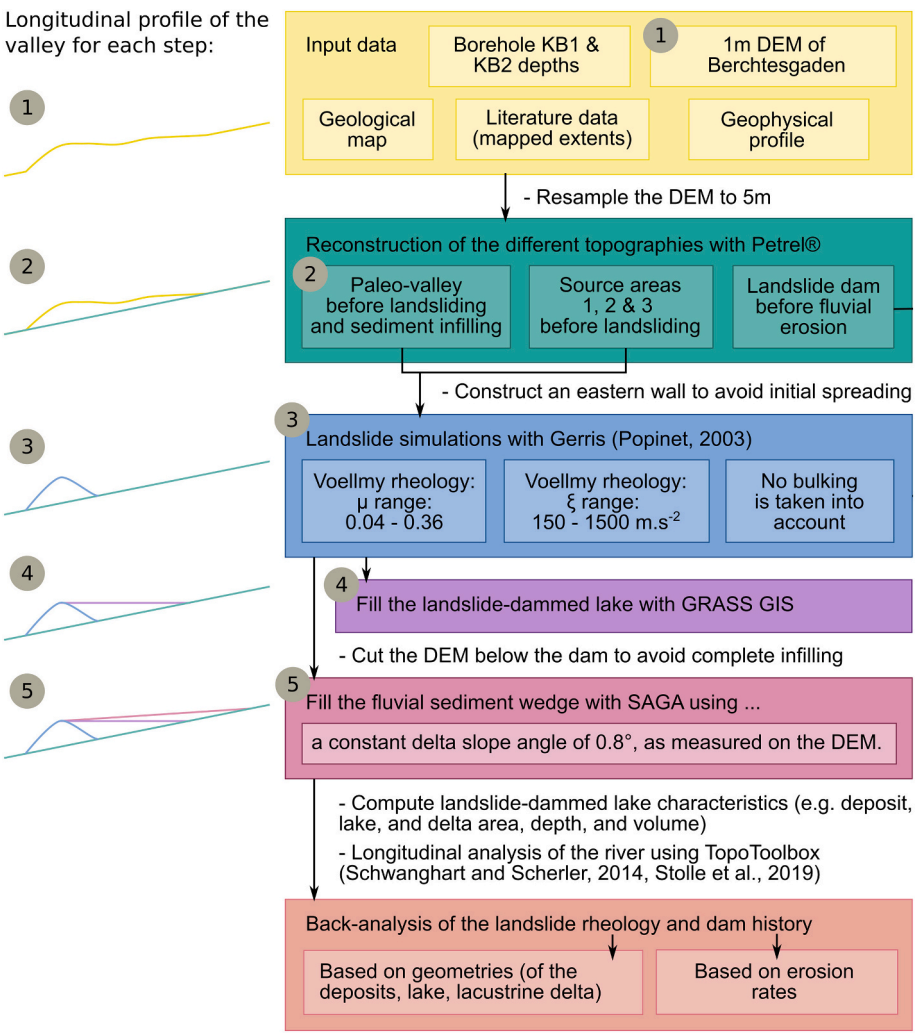

Fig. 3. Workflow of the Hintersee back-analysis, gathering the materials, methods, and model setup used to simulate the formation of a landslide-dammed lake. The longitudinal profile of the Klausbach valley is schematic.

to be reconstructed to ensure a good continuity with the topography we alter. We then draw new contour lines, longitudinal profiles, and points inside the extent to be reconstructed to modify the topography. We call these points and lines "control points/lines". We place these control points/lines based on field data (borehole depths, geophysical profile), geometric constraints (slope of the valley flanks, general shape of the valley) and geological principles (principle of continuity). To ensure a smooth and consistent transition of the reconstructed portion of the DEM with the unmodified portion, we ensure that the DEM contour lines are in continuity with the created control lines. We then combine the DEM contour lines with the control points in the same file. Using this file, we finally interpolate a surface with the convergent interpolation algorithm of Petrel®. This interpolation algorithm is used to delineate the top surface of a lithological unit in the 3D geomodelling field. It relies on a control-point orientated algorithm and iteratively converges to the solution in three steps: (1) Refine — increase the grid resolution, (2) Snap — regrid the data, (3) Smooth — minimize the grid curvature (Schlumberger, 2010). The convergent interpolation algorithm thus allows general trends to be preserved in unconstrained areas while honoring the data where they exist. The total current sediment volume (landslide and fluvial) is calculated by subtracting the pre-landslide topography from the current topography.

3.2. *Landslide runout simulation using Gerris*

For the landslide runout simulation (Fig. 3, blue), we use the Gerris flow solver (Popinet, 2003), in combination with the Voellmy rheology (Voellmy, 1955; Hergarten and Robl, 2015). Gerris is an open-source software that allows the simulation of depth-averaged granular flows. This method, close to the shallow-water equations introduced by Savage and Hutter (1989), is, among others, used by several studies to simulate debris flow and landslide runouts (Hussin et al., 2012; Schraml et al., 2015; Delaney and Evans, 2015; Lin and Lin, 2015). We opted for Gerris because of its open-source policy, its growing user community and computational efficiency (Popinet, 2003). Hergarten and Robl (2015) overcame the inherent limitation of steep terrain by solving the shallow-water equation in Cartesian coordinates by introducing several correction terms and validated their results against the leading software in the field, RAMMS (e.g., Christen et al., 2010).

We use the Voellmy rheology because, compared to the frictional and Bingham rheologies, the Voellmy rheology most accurately reproduces the debris deposition when simulating landslides with depth-averaged flow solvers (Hungr and Evans, 1996). This rheological model is characterized by only two parameters, the dry friction μ and the velocity squared drag ξ (Voellmy, 1955). The dry friction coefficient μ is defined by the ratio of the required sliding force to the force perpendicular to the topography at zero velocity. The velocity squared drag ξ consists of a density and a drag coefficient, where drag increases with velocity. These

two parameters control the resulting landslide runout and deposit geometry (Hungr, 2011): landslides with high friction coefficients tend to extend less far and form thick deposits, whereas landslides with high velocity squared drag coefficients will spread farther toward the opposite valley flank and run up higher on it.

We assume that the entire volume is released instantaneously. We do not consider sediment entrainment and bedrock loosening that could increase the volume of the detached mass. We simulate each landslide for a runout time of 6 min. Because of the high flow velocities, this duration is long enough for the rock mass to settle (i.e., for the landslide momentum to decrease to a small fraction of its maximum values). Once the simulation ends, the landslide mass is added to the DEM. The volume of sediments eroded by the river since the dam was formed is calculated by subtracting the current topography from the post-landslide topography, and summing only the positive values.

3.3. Filling the lake

To reconstruct the topography of the landslide-dammed lake after water infilling (Fig. 3, violet), the depression created in the valley by the landslide deposits is filled using GRASS GIS. The landslide-dammed lake volume is computed by subtracting the topography after landsliding from the topography after water infilling.

3.4. Filling the delta

In contrast to the infilling of a lake by water, the development of a lacustrine delta results in a slightly inclined top surface. This inclined top surface results in the delta being capable of accommodating sediment volumes of the same order of magnitude as the lake. In summary, there is an important subaerial component to the sediment trapping capacity of the landslide dam (Fig. 3, longitudinal profile 5). Therefore, we use a simple filling procedure relying on a defined minimum angle to model the sediment aggradation of the Hintersee (Fig. 3, red). 1) We extract the delta slope angle from the current topography (Fig. 3, yellow line). 2) We cut out the downstream part of the DEM at the location of the landslide dam. 3) We fill the upstream part using the Fill Sinks function of SAGA. This algorithm allows the input of a minimum fill slope threshold to preserve a minimum slope from cell to cell. We use the extracted delta slope angle of 0.8° to recreate the lacustrine delta topography. The volume of fluvial sediment is calculated by subtracting the topography after landsliding from the topography after sediment infilling.

3.5. Longitudinal profile analysis

Longitudinal profiles and their knickpoints are extracted using TopoToolbox 2.3.1 (Schwanghart and Scherler, 2014), a MATLAB add-on for topographic analysis, and its Knickpointfinder function (Stolle et al., 2019). We apply this algorithm to the same valley floor at different stages of landslide dam formation. Since the valley floor topography changes from stage to stage (e.g., damming, water infilling, sediment infilling), the flow path is also modified. Thus, the longitudinal profiles extracted for each stage do not present the same flow path, and the knickpoint propagation cannot be assessed directly from the distance to the longitudinal profile outlet. We estimate the knickpoint retreat from the planform map.

4. Model setup

The topographic evolution of the Klausbach valley can be characterized in three stages: 1) the landslide detached from the source area, leaving a scar on the valley flank, 2) the landslide settled on the valley floor and led to its infilling with fluvial sediments, 3) the landslide dam was progressively incised by the river. In this section, we explain the criteria on which we base the reconstruction of the topography as it was before each of these three stages (Fig. 3, green), and define the range of landslide rheologies that we test by back-analysis (Fig. 3, blue).

4.1. Reconstruction of the pre-landslide valley, source area and intact landslide dam

We reconstruct the valley floor prior to landslide deposition and lake sediment infilling using information from two boreholes and a longitudinal cross-section drawn from geophysical profiles (Bader, 1981). We define the maximal upstream extent of the reconstructed part by the end of the flat area in Grundübelau (extent in yellow, Fig. 1a), as suggested by von Poschinger and Thom (1995). The downstream extent is determined by examining the longitudinal profiles to obtain a smooth profile. Since the pre-landslide valley floor is known to have been imprinted by glaciers prior to the landslide, the shape we try to reconstruct is glacially-imprinted, with a widened, overdeepened valley floor. We use the boreholes from the Zauberwald area to determine the elevation of the pre-landslide valley floor in the downstream part of the valley. The longitudinal slope of the pre-landslide valley floor is given by the longitudinal profile, while the slopes of the pre-landslide valley flanks are assumed to be a continuation of the current valley flank slopes. We use two types of control lines to define the reconstructed topography: contour lines and a longitudinal profile. After interpolation in Petrel®, we fill in the reconstructed pre-landslide valley with ArcGIS to remove the depressions that formed during the reconstruction. Finally, because the landslide is modeled as a fluid from the beginning of the detachment, we add a wall on the eastern flank of the source areas to prevent the landslide mass from flowing into the adjacent valley. In reality, fragmentation of the mass only occurs during the runout and the mass only begins to behave like a fluid after some amount of travel.

In a second step, to account for the uncertainty in release volume, we reconstruct three different source areas: one based on the mapping work (extent in green, Fig. 1a) and the depths estimated by von Poschinger and Thom (1995), and two alternative areas based on the topography (Fig. 2b). The extent of the source area determined by von Poschinger and Thom (1995) is uncertain to the north, and the southern transition between the reconstructed source area topography and the current topography is not smooth. We therefore expand the source area of von Poschinger and Thom (1995) to the north in the second scenario and to the south in the third. This decision is guided by the equally flat areas on both sides of the source area of von Poschinger and Thom (1995). The extents of the new source areas are set to encompass these smooth surfaces: the northern boundary follows the ridge northward from the Steinberg peak, while the southern boundary reaches the next peak. The original slope of the source areas is assessed from the Blaueistal valley flanks, thus constraining the original elevation of the areas.

In the final step, we make a preliminary conjecture of the topography and extent of the landslide dam after landslide deposition but before fluvial erosion, before initiating any landslide simulation. We reconstruct the dam geometry based on the current topography (Fig. 4), by smoothing the current deposit surface to account for sediments removed from the landslide dam over the past 3591 ± 85 years by river incision, human construction of a pathway, and rounding of the top of the dam by hillslope processes. To constrain the former elevation, we use two areas of the landslide deposits that we believe were well-preserved over time because they were not located on the river path: to the north near the Wartstein hill, and to the south near the beginning of the Blaueistal valley. We assume that the deposits extend far downstream to the area south of the Wartstein where large boulders are scattered (Fig. 2d, e). We use the extent of the deposits mapped by von Poschinger and Thom (1995) (extent in red, Fig. 1a) as a constraint. The main depositional body formed in the middle of the Klausbach valley, at the mouth of the Blaueistal valley, probably in the form of an alluvial fan. Because the landslide flowed over the Seeklausköpfl, we presume that a second, smaller deposit area was created on the other side of the Seeklausköpfl, in the direction of the Schottmalhorn. However, reconstruction of the

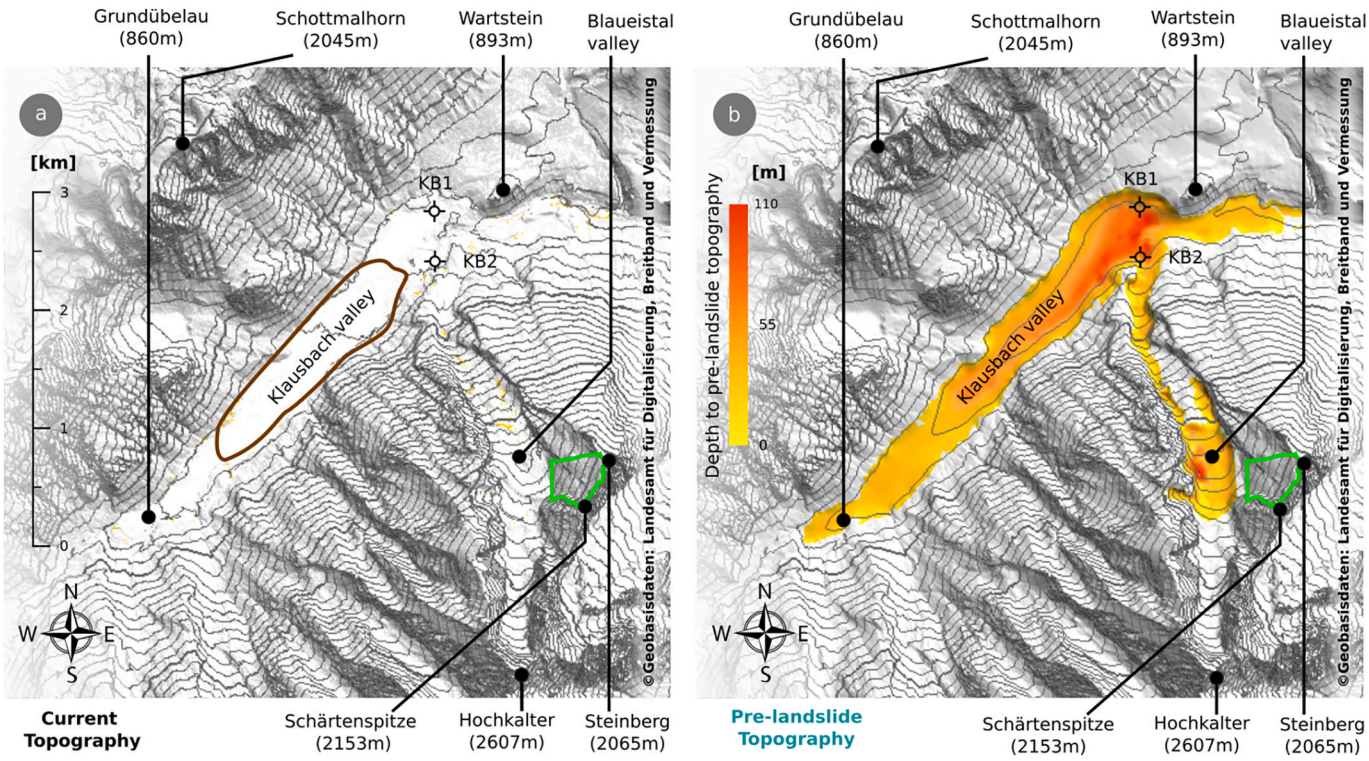

Fig. 4. 3D rendering of the Klausbach valley and the Schärtenspitze mountain before (a) and after (b) reconstruction of the valley floor using Petrel®. The locations of boreholes KB 1 and KB 2 are indicated by crosses. Isolines are drawn every 50 m. Source area 1 is outlined in green. The location of the geophysical measurements that provided a longitudinal cross-section of the pre-landslide valley floor (Bader, 1981) is outlined in brown in (a).

deposition extent to the west is uncertain due to the unknown extent of the deposits hidden by the Hintersee lake and to the east due to the dam erosion. The reconstruction of the landslide-dammed valley prior to infilling by water and sediment, or erosion, is based on the present landslide dam shape and our own conjecture of the landslide deposition extent. From this reconstruction, we calculate the thickness of the landslide dam in the Klausbach valley and the eroded thickness of the dam sediments.

4.2. Setup of the landslide rheology range

Since landslide rheology impacts the deposit geometry, we perform a back-analysis of the Voellmy rheology parameters for different source areas and volumes to find the best fit to the mapped deposits. We back-analyze the landslide-dammed lake by simulating the landslide with a range of Voellmy rheologies to test the deposit geometries. Based on the 23 rock avalanches back-analysis results from Hungr and Evans (1996) according to which ξ ranges from 100 to 1000 m.s^{-2}, and μ from 0.03 to 0.24, we vary ξ and μ from 150 m.s^{-2} to 1500 m.s^{-2} and from 0.04 to 0.36, respectively. We test each parameter combination defined in these ranges with increments of 150 m.s^{-2} for ξ and 0.04 for μ. A total of 90 different rheological combinations were tested for each of the 3 source areas, resulting in 270 simulated scenarios.

4.3. Erosion rate calculations

Erosion rates are calculated by dividing the volume of sediments found by the age of the dam. Note that the volume calculations are performed in either the Klausbach valley or the Blaueistal valley.

5. Results

We describe 1) the topographies reconstructed geometrically with Petrel®, 2) the influence of landslide rheology on the dam, dammed lake, and lacustrine delta geometries simulated using the Gerris fluid dynamics model, and 3) the back-analysis of the Hintersee lake. Finally (4)), we analyze the longitudinal profiles of the reconstructed and simulated topographies to evaluate the approach.

5.1. Topographical reconstructions

We reconstructed two topographies with Petrel®: the pre-landslide topography and the landslide-dammed valley before infilling by water and sediment, or erosion.

The reconstructed extent of the pre-landslide topography encompasses the Blaueistal valley (first landslide deposit site) and the Klausbach valley (dam site). In the Blaueistal valley, subtraction between the reconstructed pre-landslide topography and the present topography leads to a total of 27 $\times$ 10^6 m^3 of landslide deposits. The maximum sediment thickness reaches 105 m near the flank opposite of the failure area. According to our analysis, 92 $\times$ 10^6 m^3 of landslide *and* fluvial sediments were deposited in the Klausbach valley. The reconstructed area extends upstream to the Grundübelau knickpoint, and downstream to Ramsau bei Berchtesgaden (Fig. 4a). The recomputed valley floor (Fig. 4b) presents a U-shaped cross-section that is consistent with the glacial history of the valley. The thickness of the removed sediment reaches a maximum of 86 m in the middle of the Klausbach valley near the mouth of the Blaueistal valley and decreases linearly upstream and downstream. The sediment layer southwest of the Hintersee was found to be 50 m thick by Bader (1981) (geophysical profile, p. 47), which is slightly less than the average 60 m reconstructed by our topography. The total amount of sediments removed from the Blaueistal and Klausbach valleys from the present topography to create the estimated pre-landslide topography amounts to 119 $\times$ 10^6 m^3.

The three reconstructed source areas (Fig. 5) exhibit very different volumes (15 $\times$ 10^6 m^3, 44 $\times$ 10^6 m^3 and 67 $\times$ 10^6 m^3 respectively) and extents, but similar maximum thicknesses (189 m, 222 m and 232 m respectively). For comparison, the source area extent assessed by von

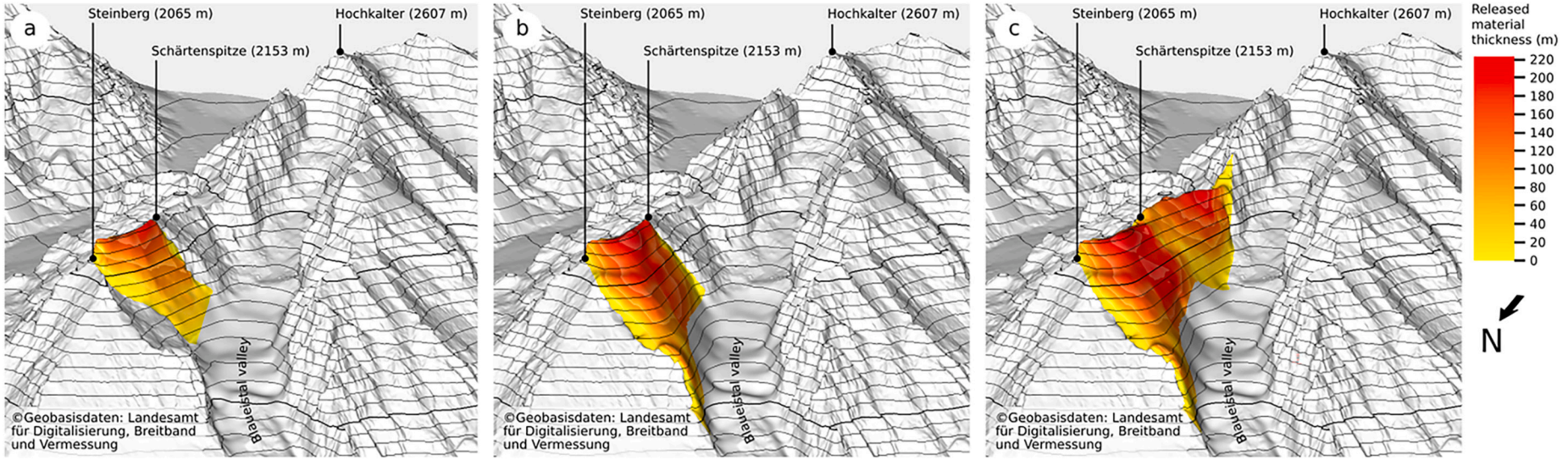

Fig. 5. 3D rendering of the three source areas reconstructed using Petrel®, displaying the differences in thickness and extent between each case: a) source area computed according to von Poschinger and Thom (1995), volume of 15×10^6 m^3, b) source area extended north of Steinberg peak, volume of 44×10^6 m^3, c) source area additionally extended further south of the Schärtenspitze, volume of 67×10^6 m^3. Isolines are drawn every 50 m.

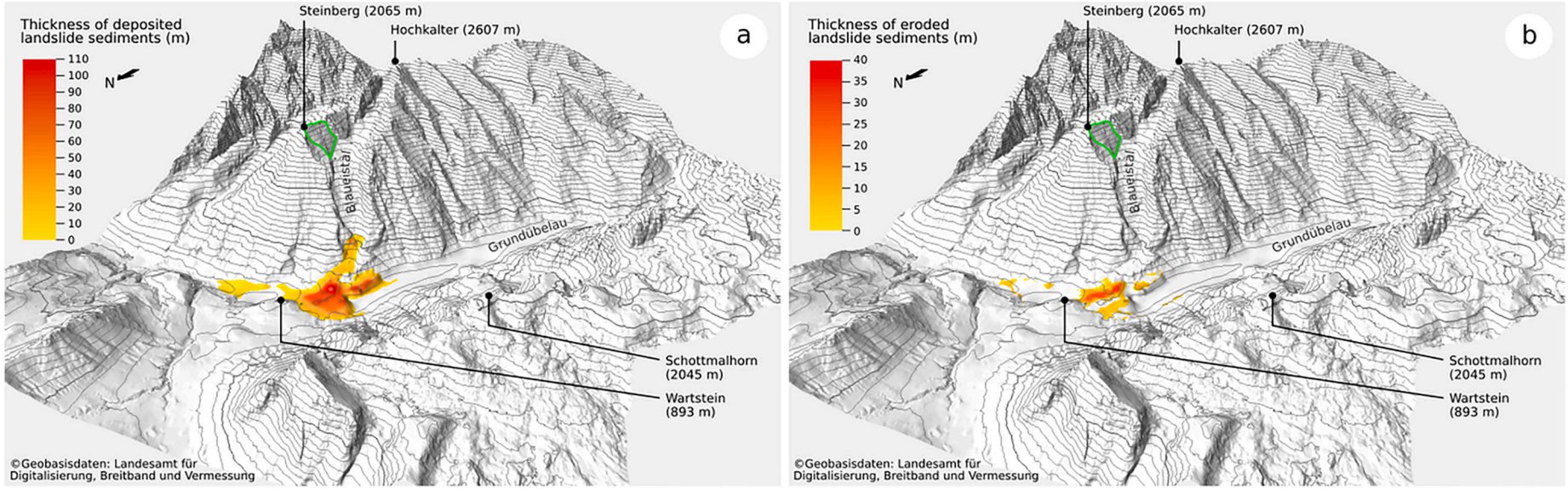

Fig. 6. 3D rendering of the landslide deposits before erosion, reconstructed using Petrel®, displaying: a) the thickness of the landslide dam relative to the reconstructed valley floor, b) the thickness of eroded sediments from the landslide dam. Isolines are drawn every 50 m. Source area 1 is outlined in green. This Petrel® reconstruction of the dam topography before erosion is based on a priori knowledge, and is not necessarily the best estimate.

Poschinger and Thom (1995), on which we based the source area 1, was estimated to support a release volume of $12 - 16 \times 10^6$ m^3. Source area 1 is flatter, and 33 m and 43 m shallower than source areas 2 and 3, respectively. In source area 1, the reconstructed valley flank below Steinberg peak is not very steep, whereas in source areas 2 and 3, the valley flank is much steeper, and Steinberg peak is located closer to the Blaueistal valley. In addition, the reconstructed material thicknesses of source areas 1 and 2 are relatively homogeneous. Source area 3, on the other hand, presents two distinct failure planes separated by the Schärtenspitze peak.

In Fig. 6a, which displays the landslide dam thickness in the Klausbach valley, the landslide mass forms a fan, with a second, smaller depositional area toward the Schottmalhorn. The total volume of sediment in the dam amounts to 32×10^6 m^3. The area of maximum depositional thickness is located near the valley flank. In comparison, the volume of sediments deposited in the Klausbach valley is estimated by von Poschinger and Thom (1995) to be $15 - 18 \times 10^6$ m^3. In Fig. 6b, which shows the eroded thickness of the dam sediments, the eroded dam sediments are mainly located along a line where the river has incised. The maximum depth of incision reaches 40 m. The volume of sediments eroded since the landslide is 4×10^6 m^3.

5.2. Influence of landslide rheology on landslide, lake, and delta geometries

Voellmy rheology parameters influence the simulated deposit geometries (Fig. 7). An increase in dry friction μ leads to narrower, therefore higher, dams and shorter runout (Fig. 7a, c, e; darkest brown), to the extent that most of the landslide mass remains stuck on the valley flank for source area 1 (Fig. 7a; darkest brown). In the high μ scenarios of source area 1, even the Zauberwald area is not completely covered by sediments (Fig. 7a), making these rheologies highly unlikely. The Brunnerlehen Mühle, where large boulders can be found in the field, is covered by deposits in half of the scenarios (for $\xi = 300$ m.s^{-2}, $\mu = 0.28 - 0.36$ for source area 1, $\mu = 0.16 - 0.36$ for source areas 2 and 3). In the source area 2 and 3 scenarios, where $\mu = 0.04$ and $\xi = 300$ m.s^{-2}, deposition extends downstream as far as Ramsau bei Berchtesgaden. In comparison, an increase in velocity squared drag ξ has little effect on the depositional area for values of ξ below 900 m.s^{-2} (Fig. 7b, d, f; darkest brown). If ξ exceeds a threshold of 900 m.s^{-2}, the deposit area increases abruptly for source areas 2 and 3 (Fig. 7d and f). The landslide extends beyond the Wartstein and landslide sediments are deposited on higher terrains on the opposite valley side. The Wartstein itself, however, is never buried under deposits. The amount of sediments deposited in the Blaueistal valley depends on μ: with $\mu = 0.04$ and $\xi = 300$ m.s^{-2}, 24.4×10^6 m^3 of landslide sediments are left in the valley, whereas the scenario $\mu = 0.36$ and $\xi = 300$ m.s^{-2} leaves only 0.2×10^6 m^3 behind. The modeled extent of landslide deposits at the Hintersee lake shows a negative linear relationship with μ and a positive non-linear relationship with ξ that relies on a threshold value.

Because the deposit geometry influences the lake formation, the lake geometry is also altered by a change of Voellmy parameters (Fig. 8). In the case of an increase in μ, the sediments are deposited closer to the valley flank, do not flow far enough into the valley floor to completely block it, and thus the lake extent decreases overall. However, the topography of the valley is not homogeneous. The valley floor is flat and wide in the upstream parts, but narrows toward the east because of the Wartstein. Depending on the defined Voellmy parameters, the landslide depositional fan adopts three different geometries conditioned by the valley topography (example in Fig. 8a). First, the landslide spreads far and reaches the opposite valley flank ($\mu = 0.04$). Second, the landslide does not reach the opposite valley flank but does reach the Wartstein, resulting in a slight increase ($\mu = 0.08 - 0.12$) and then decrease in lake area ($\mu = 0.12 - 0.24$) (Fig. B.12f). Third, the landslide only pushes the river to the side and creates small depressions without actually damming the river, inducing a distinct decrease in lake area ($\mu = 0.28 - 0.36$). By comparing the landslide deposit geometries (Fig. 7a, c, e) with the lake geometries (Fig. 8a, c, e), we can deduce the contact line between landslide sediments and impounded lake. This sediment-lake contact line evolves from a relatively straight line (Fig. 8g; red arrow) to a curved line (Fig. 8g; green arrow). For an increase in velocity squared drag ξ (Fig. 8b, d, f; darkest blue), the upstream extent of the lake remains unchanged, meaning that the dam height remains constant. However, the downstream extent of the lake is pushed upstream, and the sediment-lake contact line changes from a curved line to a relatively straight line to become curved again (Fig. 8g; red and green arrows). This change in dam-lake contact suggests that for low and high ξ, landslide sediments are heterogeneously distributed, with high thickness near the valley flank, but are deposited more evenly across the valley floor for medium ξ values. In summary, μ exhibits a non-monotonic relationship with the extent of Lake Hintersee that is driven by the valley topography (e.g., the presence of the Wartstein), as is the case for the extent of landslide deposits. As for ξ, the extent of Lake Hintersee is relatively insensitive to it in the upstream part, but shows a non-linear relationship with ξ in the downstream part.

Finally, the landslide rheology also impacts the extent of the lacustrine delta formed upstream of the landslide-dammed lake (Fig. 9). For the same velocity drag squared coefficient ξ of 300 m.s^{-2}, the delta area for the source area 1 scenario augments by 0.8% between $\mu = 0.04$ and $\mu = 0.08$, then decreases by 6.2% between $\mu = 0.08$ and $\mu = 0.36$. For source area 2, the delta area increases by 2.0% between $\mu = 0.04$ and $\mu = 0.12$, then decreases by 11.0% between $\mu = 0.12$ and $\mu = 0.36$. For source area 3, it increases by 2.1% between $\mu = 0.04$ and $\mu = 0.12$, then decreases by 13.0% between $\mu = 0.12$ and $\mu = 0.36$. The shape of the sediment infill is similar to the lake extent. The velocity drag squared coefficient ξ does not greatly influence the lacustrine delta area (Fig. 9b, d, f). For the same dry friction μ of 0.08, the delta area oscillates around $6.41 \pm 0.02 \times 10^6$ m^2, $6.675 \pm 0.025 \times 10^6$ m^2, and $6.81 \pm 0.04 \times 10^6$ m^2 for source areas 1, 2, and 3, respectively.

In terms of volumes, areas and depths of deposits, lakes, and lacustrine deltas (Fig. 10), the impact of landslide rheology depends again more on dry friction μ than velocity drag squared coefficient ξ. With increasing μ, the dam gets higher (Fig. 10b) and forms steeper flanks, while the deposit area decreases (Fig. 10a). In contrast, the volumes, areas, and depths of the lake (Fig. 10e, f, g) and delta (Fig. 10h, i, j) increase only up to a certain μ threshold, and then decrease. This threshold is influenced by the velocity drag squared coefficient ξ.

For high friction coefficients μ, landslide deposits reach a larger maximum thickness, but are less homogeneously distributed over the valley floor. This leads to relatively shallower landslide-dammed lakes, with the example of the source area 1, $\mu = 0.36$, exhibiting a lake with a maximum depth of 2 m and an average depth of <1 m.

5.3. Best-fit scenario

We assess which scenario is most appropriate for the Hintersee landslide event in terms of release volume and landslide rheology from the landslide deposit, dammed lake, and delta planform (Figs. 7, 8, and 9) and cross-sectional geometries (Fig. 10).

With respect to release volume, source areas 2 and 3 give the best fits for the extent of deposits and lake (Figs. 7 and 8, respectively). We assume that the former area of the Hintersee lake includes the entire extent of the current lake (blue, Fig. 8). By examining the simulated lake extents and the location of the present-day Hintersee lake, we find that source area 2 is a minimum requirement in terms of depositional volume and height to reach the lake extent that explains the northern border of the current Hintersee lake. The same can be said to achieve the mapped deposit extent (yellow, Fig. 7). Source area 1 is thus not sufficient to create a deposit thickness compatible with the borehole depths of 37 m of KB1 (Fig. B.12c), contrary to source areas 2 and 3 (Fig. 10c).

As for the Voellmy rheology coefficients, $\xi = 300$ m.s^{-2} and $\mu = 0.08$ seem to give the best fits to the extent of the lake (Fig. 8). While the low μ

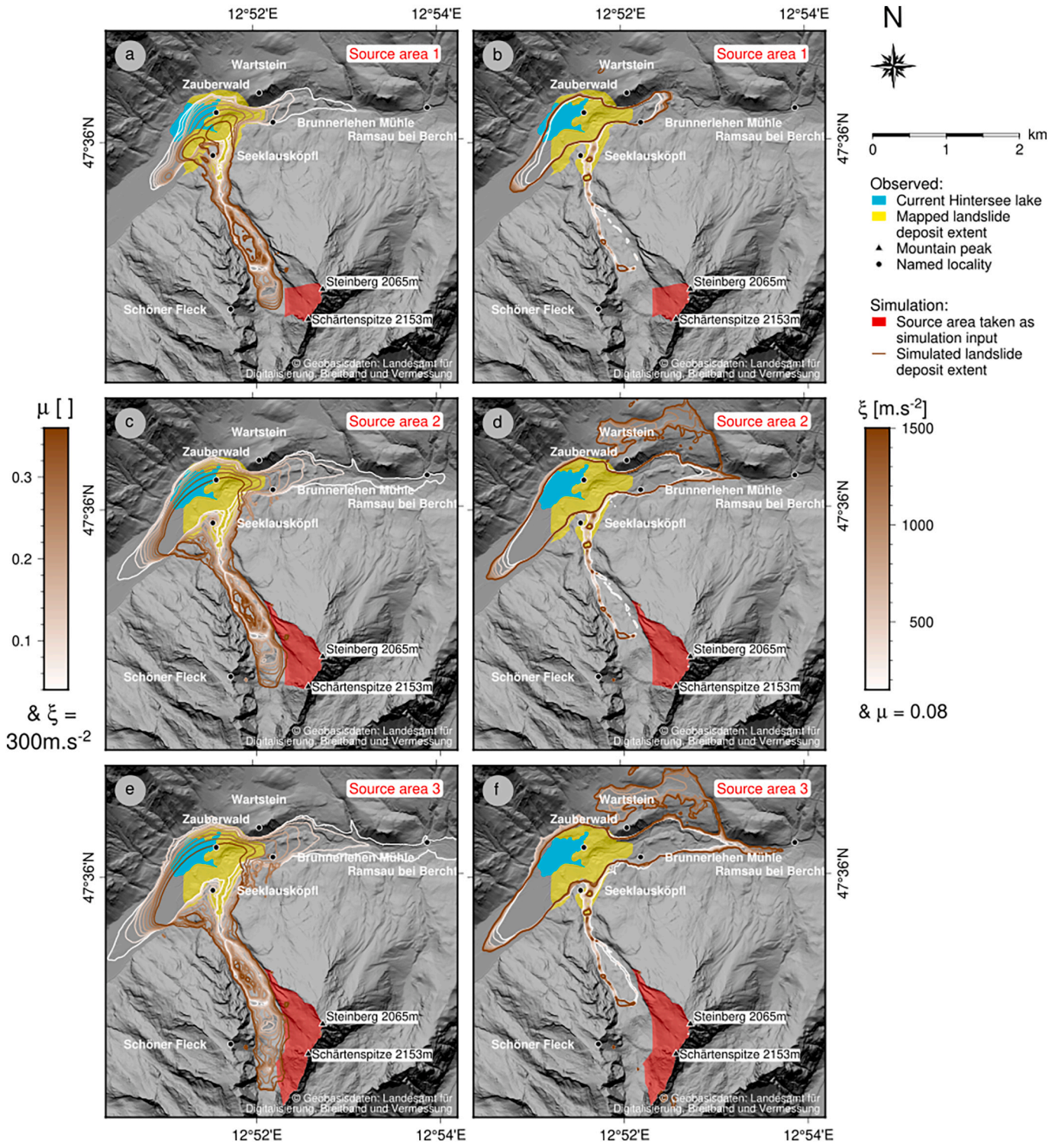

Fig. 7. Influence of the Voellmy rheology parameters μ and ξ on the geometry of the landslide deposit for all three source areas. For varying μ, ξ set to 300 m.s^{-2}: a) Source area 1, c) Source area 2, e) Source area 3. For varying ξ, μ set to 0.08: b) Source area 1, d) Source area 2, f) Source area 3. The landslide deposit boundaries are plotted as solid lines in shades of brown, reflecting the value of the variable rheology parameter. Landslide deposit pixels are considered inside the deposit area if the deposit thickness exceeds 1 m. The mapped landslide deposits are plotted in yellow. The current Hintersee lake is displayed in blue. We focus on the $\xi = 300$ m.s^{-2} and $\mu = 0.08$ scenario as we determine it to be the best-fit scenario (Section 5.3). Further scenarios are shown in the Supplementary.

scenarios display better fits to the deposit extent in the Zauberwald, they also stretch far downstream, reaching Ramsau bei Berchtesgaden. The velocity squared drag ξ, on the other hand, does not impact the upstream and downstream depositional extent very much, although high values allow sediments to reach the opposite valley flank (which is not the case in the field, however). The borehole KB1 tends to indicate coefficients of $\xi = 300$ m.s^{-2} or higher and $\mu = 0.08$ (Fig. B.12c).

We note that even in the simulations giving the largest lake extents, the lake does not reach the upper part of the reconstructed valley, the Grundübelau, but that the deposit extent predicted by von Poschinger

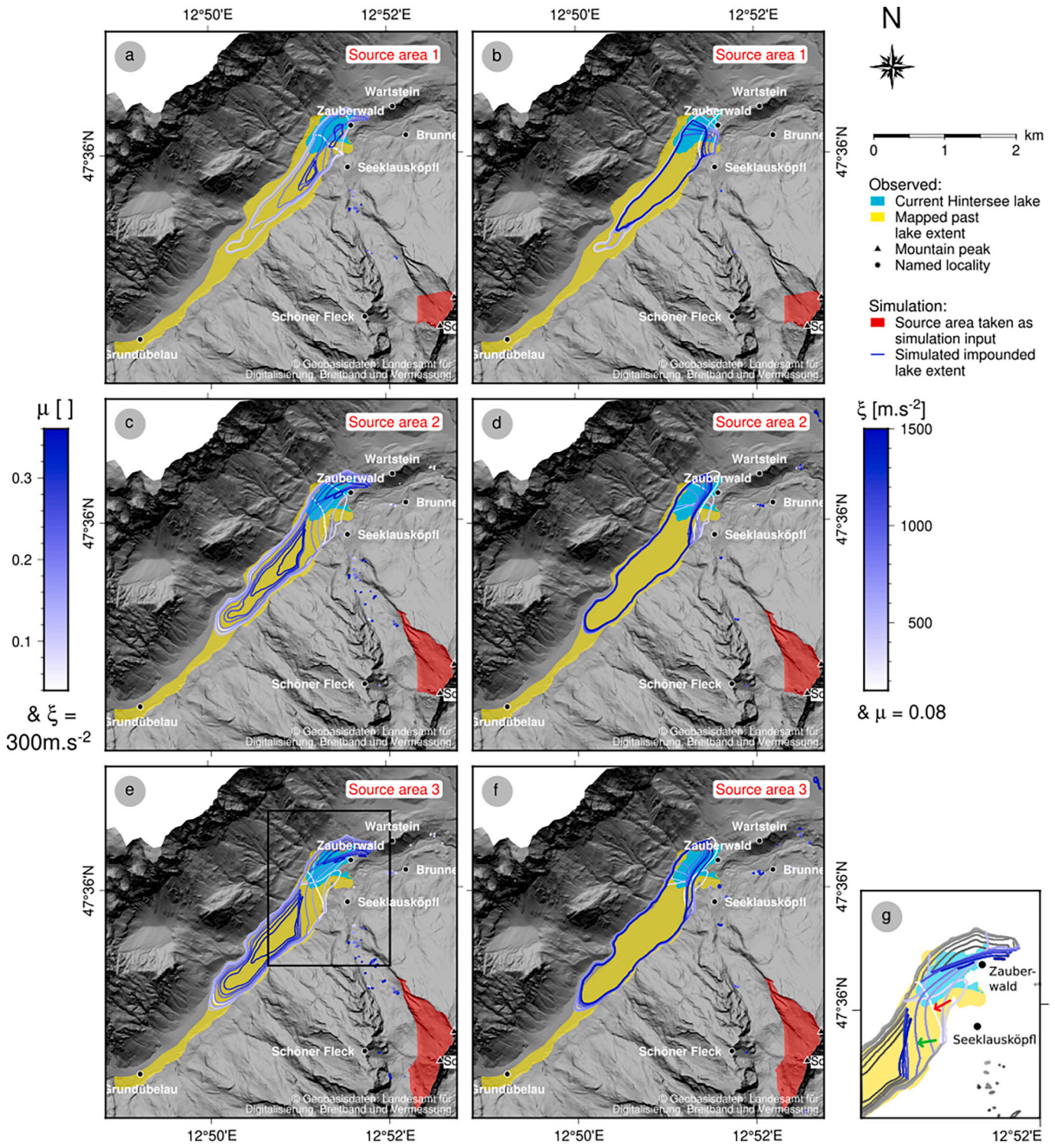

Fig. 8. Influence of the Voellmy rheology parameters μ and ξ on the geometry of the landslide-dammed lake for all three source areas. For varying μ, ξ set to 300 m.s^{-2}: a) Source area 1, c) Source area 2, e) Source area 3. For varying ξ, μ set to 0.08: b) Source area 1, d) Source area 2, f) Source area 3. The landslide-dammed lake boundaries are plotted as solid lines in shades of blue, reflecting the value of the variable rheology parameter. Lake pixels are considered inside the impoundment area if the lake depth exceeds 1 m. g) highlights the sediment-lake contact lines in a zoom-in of e). The inferred lake sedimentation area is plotted in yellow. The current Hintersee lake is displayed in blue. We focus on the $\xi = 300$ m.s^{-2} and $\mu = 0.08$ scenario as we determine it to be the best-fit scenario (Section 5.3). Further scenarios are shown in the Supplementary.

and Thom (1995) is exceeded in the favored scenarios. However, the extent of the flat area upstream of the knickpoint can be explained by the delta of fluvial sediments formed behind the landslide dam. We therefore conclude that the best scenario for the Hintersee landslide is a deposit volume at least equal to source area 2, and with Voellmy rheology coefficients $\mu = 0.08$ and $\xi = 300$ m.s^{-2}.

5.4. Validation by analysis of the longitudinal profiles of each topography

In Fig. 11a, we can see the flow paths computed on the current

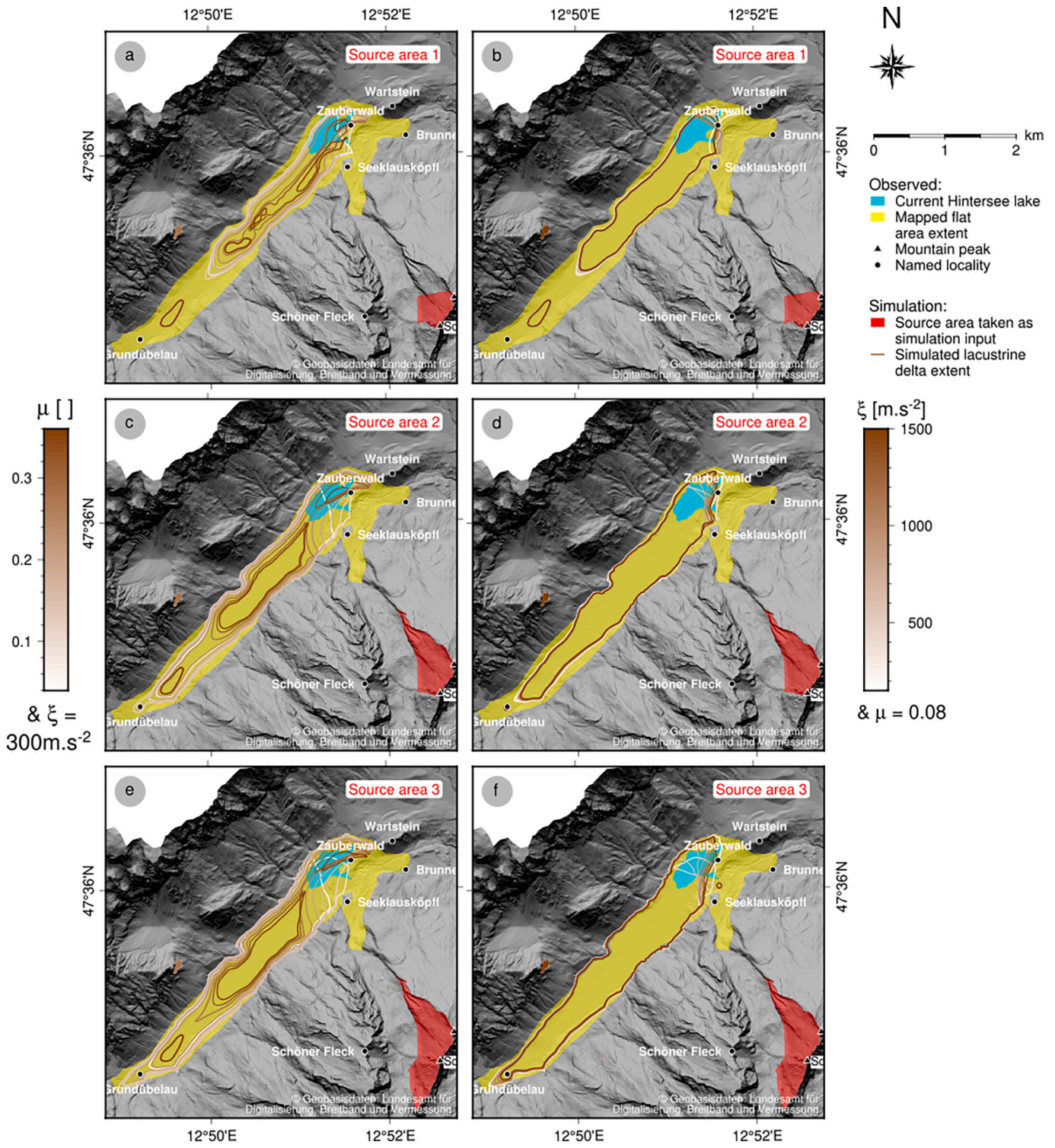

Fig. 9. Influence of the Voellmy rheology parameters μ and ξ on the geometry of the lacustrine delta for all three source areas. For varying μ, ξ set to 300 m.s^{-2}: a) Source area 1, c) Source area 2, e) Source area 3. For varying ξ, μ set to 0.08: b) Source area 1, d) Source area 2, f) Source area 3. The lacustrine delta boundaries are plotted as solid lines in shades of brown, reflecting the value of the variable rheology parameter. Delta pixels are considered inside the deposit area if the deposit thickness exceeds 1 m. The inferred lake sedimentation area is plotted in yellow. The current Hintersee lake is displayed in blue. We focus on the $\xi = 300$ m.s^{-2} and $\mu = 0.08$ scenario as we determine it to be the best-fit scenario (Section 5.3). Further scenarios are shown in the Supplementary.

topography and the four reconstructed and simulated topographies: the flow path of the current topography (black) follows the SE valley flank, while the flow path of the pre-landslide topography (cyan) goes through the middle of the valley. The river is pushed to the side, in an avulsion, by the landslide deposits (red - disappearing under the cyan pre-landslide flow path). The water infilling of the depression (blue) moves the flow path to the center of the created lake, as does the sediment infilling of the depression (orange).

In Figs. 11b and c, we observe the longitudinal profiles of the current topography, of the reconstructed pre-landslide topography and of two

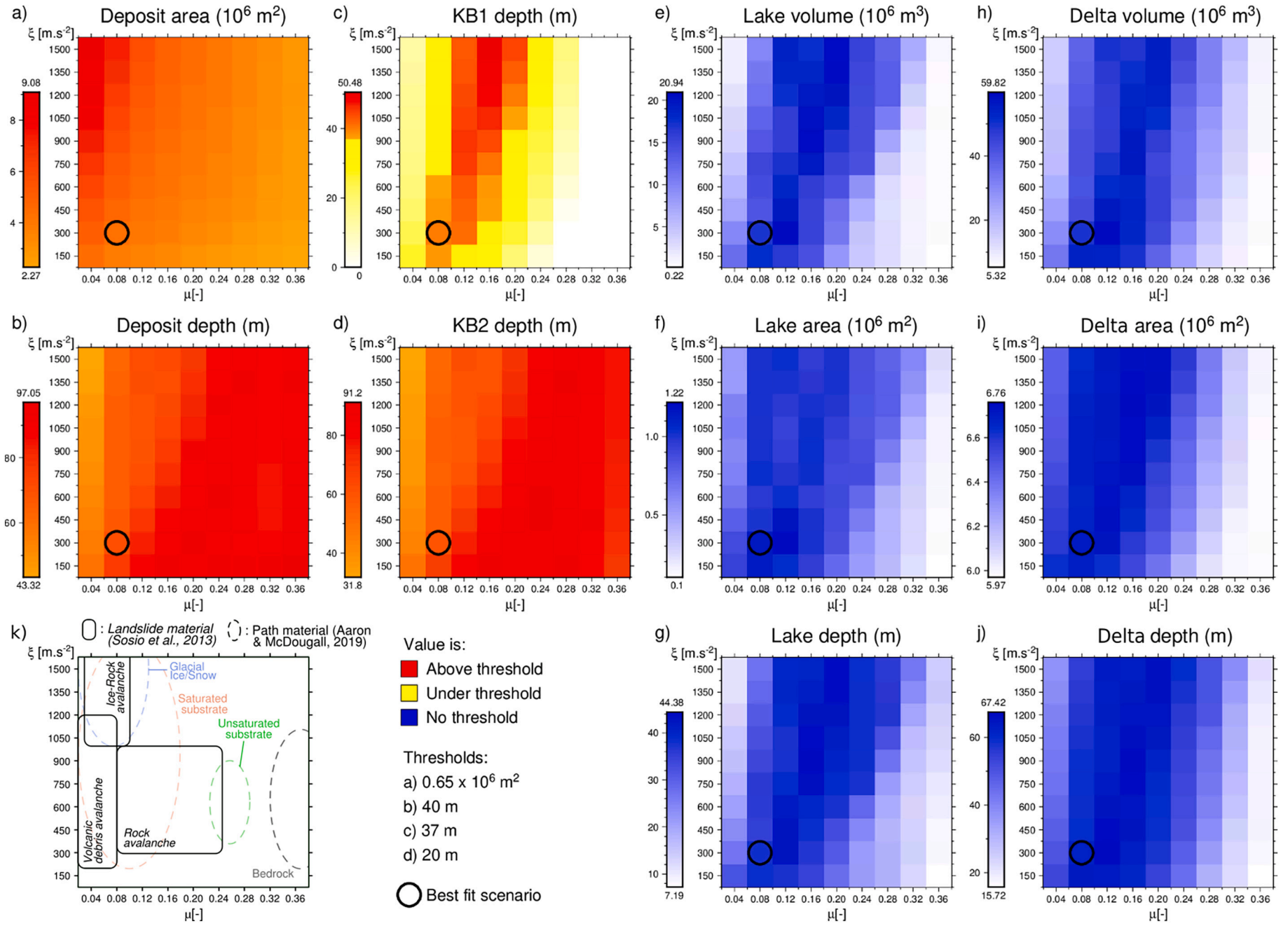

Fig. 10. Influence of the Voellmy parameters (i.e., the dry friction μ and the velocity squared drag ξ) on the geometries of the landslide dam (a-d), landslide-dammed lake (e-g), and lacustrine delta (h-j) for source area 2. Values are plotted using a color gradient and compared to indicative thresholds when available: a) the area and b) depth of landslide deposit predicted by von Poschinger and Thom (1995), c) the minimum landslide deposit depth found in borehole KB1 and d) KB2 by Risch (1993). Values above the thresholds are plotted in red, those below in yellow, and those without indication in blue. The best fit scenario found based on the plan and cross-section geometries is highlighted by a circle. k) represents the known landslide lithologies and landslide path characteristics.

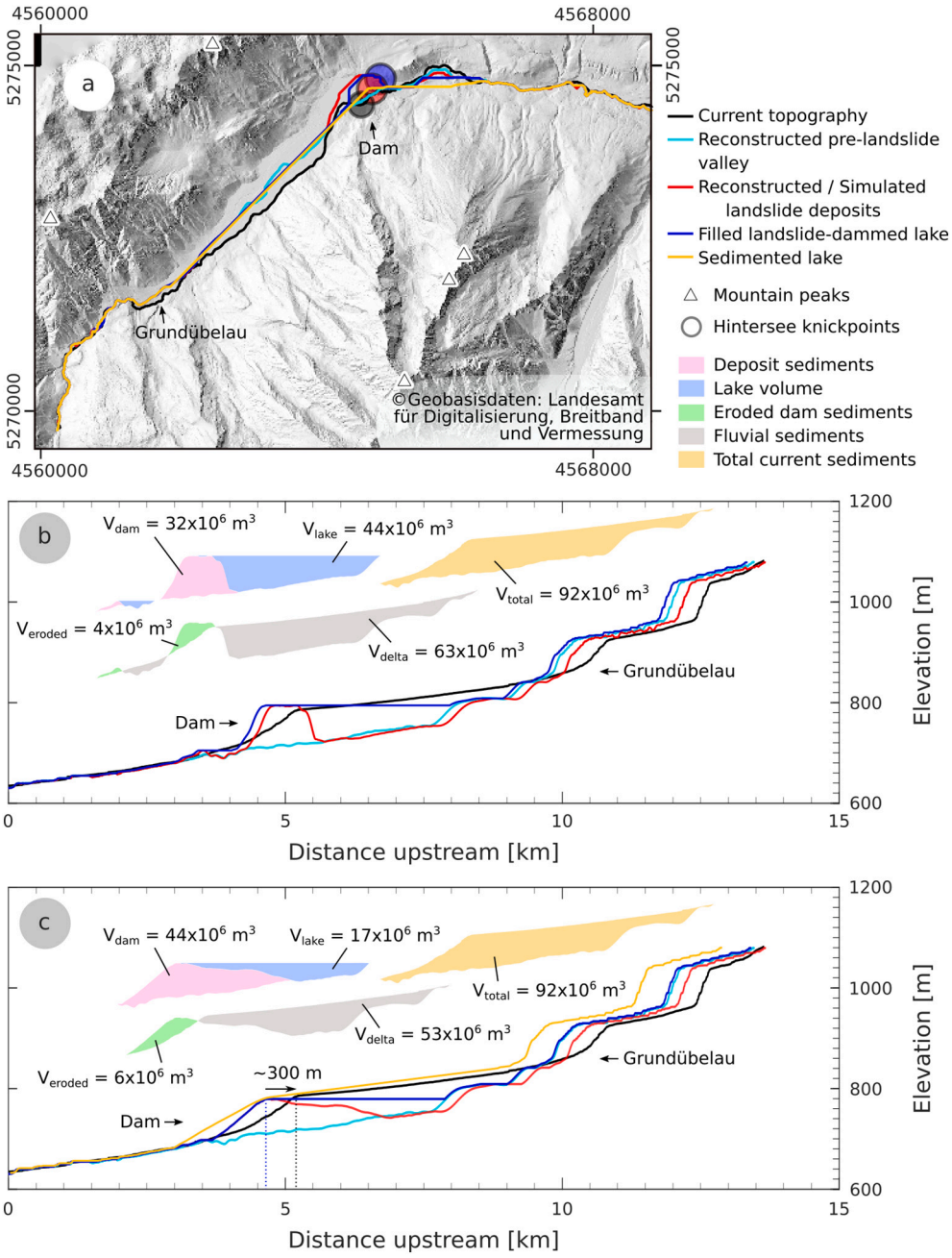

Fig. 11. Comparison of the longitudinal profile of the Klausbach river for the current topography (in black), the reconstructed topography before landsliding (in cyan), the topography after landsliding (in red), after water infilling (in blue) and sediment infilling (in orange). a) Traces of the longitudinal profiles on the valley floor, with location of the Hintersee knickpoints. Since the topography changes, the flow path also changes for each topography. These differences in flow paths explain some of the shifts in the longitudinal profiles (b & c). b) Longitudinal profiles for the landslide deposits as reconstructed using Petrel® based on the mapped extent of landslide deposits. c) Longitudinal profiles for the landslide deposits as simulated with Gerris in the best-fit scenario (Source Area 2, Voellmy coefficients μ = 0.08 and ξ = 300 m.s^{-2}). The volumes of different parts of the dam and dammed lake found in the Klausbach valley are indicated using fills.

scenarios of the landslide dam, one geometrically reconstructed with Petrel®, and the other simulated using the Gerris fluid dynamics model. The pre-landslide valley exhibits a relatively constant delta slope angle of approximately 0.8° from the origin of the plot to a bump just below the Grundübelau knickpoint. This bump, although a modeling artifact (cf. Discussion), respects the overall slope of the valley. This slope of 0.8° is consistent with the slope of the delta measured on the current topography, which contributes to its validation.

In the Klausbach valley, the total amount of sediment removed from the current topography to reconstruct the pre-landslide topography reaches V_{total} = 92 × 10^6 m^3 (orange areas, Fig. 11c, d). This volume comprises the landslide sediments from the dam and the fluvial sediments deposited upstream of the dam.

We can compare the reconstructed dam topography (red line, Fig. 11b) with the simulated dam topography (red line, Fig. 11c). Although the dam reconstructed using Petrel® based solely on a priori knowledge presents a lower dam volume V_{dam} = 32 × 10^6 m^3 (red area, Fig. 11b) than the simulated dam (V_{dam} = 44 × 10^6 m^3 (red area, Fig. 11c), the dam is much higher, thus impounding a much bigger lake (blue areas, Fig. 11b and c). This reconstructed dam also extends much less downstream and upstream, which leads to a smaller volume of sediments already eroded from the dam (green areas, Fig. 11b and c).

The sediment trapping capacity of the dam V_{delta}, i.e., the maximum volume of sediment that can be stored in the sediment trap (gray areas, Fig. 11b and c), exceeds the maximum volume of trapped water V_{lake} (blue areas, Fig. 11b and c). This difference in volume is due to a contrast in surface geometry: fluvial sediments are deposited at a positive delta slope angle, while a water body presents a flat surface. In the best-fit scenario, the simulated lake is relatively shallow, with V_{lake} = 17 × 10^6 m^3 (blue area, Fig. 11c), while the volume of fluvially accumulated

sediments $V_{delta} = 53 \times 10^6$ m^3 (gray area, Fig. 11c) reaches more than three times the volume of water.

Sediment is trapped upstream of the dam, but the dam itself is eroded by the river and releases sediments in it. By subtracting the current topography to the simulated landslide deposits in the region of the dam, we obtain an eroded dam volume V_{eroded} of 6×10^6 m^3 (green area, Fig. 11c).

The landslide dam forms a knickpoint (Fig. 1c) in the longitudinal profile of the river. We compare the position of the knickpoint on the current topography and on the reconstructed topography after landslide damming. This knickpoint is moving upstream while the dam gets eroded and the volume of eroded sediments increases.

6. Discussion

This study back-analyzed the formation of the Hintersee landslide-dammed lake by simulating a range of landsliding scenarios with variable landslide rheologies and release areas. In the following subsections, we discuss the uncertainties and simplifications in the employed methodology, the impact of landslide rheology on the formation and capacity of landslide-dammed lakes and their associated sediment storage, the a priori bias on landslide dam geometry and the Hintersee landslide dam history.

6.1. Uncertainties and simplifications

The biggest limitations of our approach originate from 1) uncertainties in the reconstruction of the pre-landslide topography including (a) valley floor where the landslide settled and (b) valley flank where the landslide originated, 2) the omission of landslide bulking, and 3) the simplification of landslide rheology.

There is a relatively high uncertainty on the reconstruction of the pre-landslide valley topography (Fig. 4), due to imprecise information and partial constraints. The geophysical profile indicates only a rough thickness of the lake sediments, and as the boreholes did not reach the bottom of the lake sediment layer, they provide only a minimum deposit thickness. Furthermore, although we validated the pre-landslide valley topography using longitudinal profiles, the profile is irregular and exhibits a slight bump close to the Grundübelau knickpoint. These irregularities are intrinsic to the reconstruction method used. However, this unevenness is small-scale and has a negligible impact on volume computations in comparison with the overall uncertainty due to the absence of precise depth information.

A higher uncertainty is present for the pre-landslide valley flank topography. Contrary to the valley floor, no release mass thickness can be measured. The only hints for the estimation of the released volume are the current valley flank topography and the deposited landslide volume in the Klausbach valley. Thus, we reconstructed three source area topographies (Fig. 5) to take into account the uncertainty linked to the source area extent and release volume. In the three cases, we observe the same simulated landslide path. Thereby, we can extrapolate the release volume from the deposit geometries without worrying about the influence of the source area geometry on the end result.

We simulated landsliding with three source areas of increasing release volumes and found that the best fit in terms of source area for the deposit extent is the intermediate scenario, with a release volume of 44×10^6 m^3 (Fig. 7c, d). However, we did not account for sediment bulking due to fragmentation or entrainment during the runout. Von Poschinger and Thom (1995) commonly use a bulking factor of 1.3, although this value is highly uncertain, with studies constraining a range from 7 to 26% of volume increase due to fragmentation (e.g., Hungr and Evans, 2004), and a measured porosity of 18 to 35% in landslide deposits. Thus, if we assume a bulking factor of 1.3, the release volumes of the three source areas are reduced to 11.5×10^6 m^3, 33.8×10^6 m^3 and 51.3×10^6 m^3. Although the corrected release volume of source area 1 is consistent with the release volume determined at $12 - 16 \times 10^6$ m^3 (von Poschinger and Thom, 1995), the simulations predict a required release volume of 33.8×10^6 m^3 to form a deposit of the extent of the Hintersee landslide dam and create a lake of the size of the Hintersee lake.

To investigate the influence of landslide rheology on the geometry of the landslide deposit, we tested a set of Voellmy rheologies (Fig. 10) and found that $\mu = 0.08$ and $\xi = 300$ m.s^{-2} leads to a landslide deposit that is largely consistent with the geometry of the observed deposit at the Hintersee lake. However, the landslide rheology may change spatially (e.g., different rock types in a single landslide) or temporally (e.g., material entrainment during the runout, fragmentation, water content change; Hungr, 2011; Shen et al., 2019). Thus, our rheological model is simplified by neglecting spatial and temporal variations in fluid rheology.

6.2. Impact of landslide rheology on landslide damming and sediment trapping

For a given valley geometry, landslide rheology is a key controlling factor in the formation of a landslide-dammed lake (Fig. 8).

A low friction coefficient will create a flat dam with little impoundment, while a high friction coefficient can prevent the landslide from reaching the river or from spreading laterally enough to dam the river (Fig. 7a). Thus, landslide rheology is a non-linear controlling factor on lake and delta geometries (Figs. 8, 9).

The influence of landslide rheology is mitigated by valley geometry. When testing different Voellmy rheologies on a set of 10 cases, Argentin et al. (2021) showed that the results were not consistent. In four cases, an increase of dry friction resulted in a non-linear, but continuous, change of lake volume. However, this trend change did not occur for the same friction thresholds or in the same directions for all four cases.

Landslide rheologies depend, among others, on landslide lithology (Sosio et al., 2013; Zimmermann et al., 2020), path material (Aaron and McDougall, 2019) and, potentially, water content (Naaim et al., 2013). Rock avalanches ($\mu = 0.08 - 0.25$ and $\xi = 300 - 1000$ m.s^{-2}) exhibit medium to high friction coefficients, while volcanic debris avalanches ($\mu = 0.003 - 0.08$ and $\xi = 200 - 1200$ m.s^{-2}) are characterized by low friction and ice-rock avalanches ($\mu = 0.03 - 0.1$ and $\xi = 1000 - 2000$ m.s^{-2}) by long runouts (Sosio et al., 2013). The variable μ is correlated positively with clay content, but not with water saturation or other soil physical properties (Zimmermann et al., 2020). On the relation of path material to Voellmy rheology coefficients (Aaron and McDougall, 2019), rock avalanches overrunning glacial ice/snow ($\mu = 0.03 - 0.13$ and $\xi = 1000 - 2100$ m.s^{-2}) display the highest mobility (Zimmermann et al., 2020), followed by rock avalanches with saturated substrate ($\mu = 0.05 - 0.18$ and $\xi = 200 - 1700$ m.s^{-2}), those with unsaturated substrate ($\mu = 0.23 - 0.29$ and $\xi = 350 - 900$ m.s^{-2}), and rock avalanches overrunning bedrock that display the highest motion resistance ($\mu = 0.32 - 0.45$ and $\xi = 200 - 1100$ m.s^{-2}). Higher friction coefficients could be obtained by landslides with very coarse debris substrate (e.g., Val Pola and Hope, Aaron and McDougall, 2019). Thus, water content increases the mobility. This finding is backed up by similar results reported for debris flows (Hürlimann et al., 2015), and snow avalanches (Naaim et al., 2013) where the friction is linked negatively to water content above a certain water threshold.

Since landslides with high friction coefficients have lower chances of damming rivers, unsaturated substrate landslide have lower chances of

forming big lakes and deltas.

6.3. A priori reconstruction

There is a significant difference between the geometry of the dam geometrically reconstructed with Petrel® using a priori knowledge only (Fig. 11b), and the geometry of the dam simulated using the Gerris fluid dynamics model (Fig. 11c). Although both dam reconstructions are empirically constrained at certain locations (e.g., boreholes), the depth-averaged flow simulation with Gerris allows for physics-based constraints (e.g., friction, depositional angles) on the possible geometries of the dam to be introduced. Whereas the a priori reconstruction using Petrel® relies on expert based knowledge, making it prone to misjudgment and bias (Bond, 2015). Thus, the reconstruction of the dam based on landslide deposit remains using Petrel® generally leads to an overestimation of the dam height and an underestimation of its extent in downstream and upstream direction. The extents upstream and downstream are not easily recognizable in the field, which is common for old, sediment covered or eroded landslide dams. This appraisal error leads to questioning the uncertainty (Bond, 2015) linked to dam geometry assessments.

6.4. Back analysis of the Hintersee landslide dam

The best fit of the landslide rheology back-analysis was achieved with $\mu = 0.08$ and $\xi = 300$ m.s^{-2} (Fig. 10). Some studies found that this set of rheological parameters is suitable for volcanic debris, but also for rock avalanches (Fig. 10k; Sosio et al., 2013), hints toward a low clay content (0–5%, Zimmermann et al., 2020) and is characteristic of a water-saturated substrate (Fig. 10k, red; Zimmermann et al., 2020), which could indicate a rainfall-trigger. According to these studies, the Hintersee landslide would thus have occurred as a rock avalanche with low clay content and would have run on a water-saturated substrate. The two first assumptions can be easily defended, as the source lithology of the Hintersee landslide consisted of carbonatic rocks, and the mass deposited relatively close to its source, with large blocks found in the Klausbach valley. The third assumption is harder to validate, although it is partly supported by the conclusions drawn by von Poschinger and Thom (1995) about the absence of snow cover. Since temperatures at the time of the landslide were higher than in 1819 (Ilyashuk et al., 2011), when the end moraine only reached the upper parts of the Blaueistal valley (von Poschinger and Thom, 1995), a glacier of greater extent would have been very unlikely and the substrate would not have been covered with snow or ice. This would only leave a water-saturated substrate to explain the low friction of the landslide. However, this speculation about the climatic conditions at the time of triggering remains uncertain.

6.4.1. Erosion and stability of the landslide dam - a possible partial breach

Since most of the sediments from the Hintersee landslide are still present in the field, we can deduce that the Hintersee landslide dam did not undergo a full failure. However, a gradual erosion of the Hintersee landslide dam by the Klausbach river is debated. Von Poschinger and Thom (1995) advance the hypothesis of a partial catastrophic outburst, based on the boulders found downstream of the dam and channels found in the deposits. However, according to the best fit scenario of our model, the landslide deposit extends much farther downstream than recognizable in the terrain today (Fig. 7). Hence, these large boulders could mark the actual extent of the landslide instead of giving evidence for a dam break and flooding. On the other hand, the simulation output indicates that the volume of landslide dam sediments already eroded reaches 6×10^6 m^3 (Fig. 11c). In the case of a gradual erosion, this volume implies a mean erosion rate of ~1,600 m^3.yr^{-1} over the last 3591 years, a maximum erosion rate of 7930 mm.ka^{-1} at the deepest incised point and a mean erosion rate of 850 mm.ka^{-1} over the whole dam. These numbers are well under bedrock incision rates reported from cases of landslide-induced river avulsions (Pratt-Sitaula et al., 2007). Furthermore, by comparing the position of knickpoint on the current topography and on the reconstructed topography after landslide damming (Fig. 11), we find that the Hintersee landslide dam knickpoint moved approximately 300 m since landsliding, thus entailing a mean knickpoint migration velocity to 0.08 m.yr^{-1} over the last 3591 years.

6.4.2. Sedimentation of the landslide-dammed lake

The landslide-dammed lake of the Hintersee does not reach as far upstream as the lacustrine delta and has a smaller volume (Fig. 11). According to the simulated lake and delta geometries (Figs. 8, 9), and contrary to the assumptions of von Poschinger and Thom (1995), we suggest that the landslide-dammed lake did not reach the upper part of the valley, the Grundübelau. In fact, the knickpoint observed in Grundübelau matches the upper extent of the fluvial sediment aggradation, while the former upper extent of the dammed lake cannot be determined easily from topographic data. According to the longitudinal profiles (Fig. 11c), only one third of the fluvial sediments are trapped in the dammed lake itself, while two thirds are stored into the lacustrine delta formed upstream due to the creation of a new base level. Thus, we suggest that studies taking landslide-dammed lake volume as a proxy for sediment trap capacity are underestimating the impeding action of landslide dams on sediment transport, and should use a correction coefficient.

By taking the volume of trapped sediments (gray area, Fig. 11c), the time since the landslide happened, the upstream area, as well as the densities of the solid bedrock and unconsolidated sedimentary infill, we can roughly deduce the mean denudation rate of the catchment and sedimentation accumulation rate in the lake (Hinderer, 2001). This approach is subject to some uncertainty since the Hintersee and the upstream Klausbach river have been subject to man-made modifications to avoid the complete sediment infilling of the lake. The upstream area and the age of the landslide are well-constrained, but the volume of trapped sediments has a higher uncertainty. According to the best fit scenario, the volume of trapped sediments solely in the Klausbach valley amounts to $V_{delta} = 53 \times 10^6$ m^3 (gray area, Fig. 11c). We take a solid bedrock density of 2.5 g.cm^{-3} and a density of unconsolidated sedimentary infill of 1.7 g.cm^{-3} (Hinderer, 2001), which leads to a mean denudation rate of 230 mm.ka^{-1}, which is well in line with erosion rates reported for formerly glaciated alpine catchments (Delunel et al., 2020).

These volumes and erosion rates are linked to the valley gradient. In the Klausbach valley, the local slope upstream of the Hintersee dam is spatially variable (Fig. 11c, black). Near the Grundübelau, the creation of a local base level probably triggered sediment deposition, in a manner similar to alluvial fans, with high slopes (usually between 1.5° and 25°; Blair and McPherson, 1994; Crosta and Frattini, 2004), while downstream, closer to the Hintersee, the remainder of the sediments were deposited in a flatter fashion, more characteristic of fluvial processes (Blair and McPherson, 1994). These sedimentation slope values vary greatly depending on the location of the landslide dam in the mountain range. Indeed, the local slope is related to the longitudinal profile of the river (Hack, 1957). Landslide dams located farther downstream would be filled with a significantly lower alluvial gradient. At a smaller scale, the local gradient is also sensitive to the type of sedimentation process, the river regime (e.g., suspended-sediment, mixed-load, and bedload transport), and the sediment characteristics (e.g., grain size and shape,

lithology) (Dade and Friend, 1998). However, a lower sedimentation slope does not guarantee that a smaller volume of sediment will be trapped, as the valley slope will also be lower, providing a larger accommodation space.

As long as a landslide dam blocks the water flow, most of the fluvial sediments are trapped. The water seeps through the dam and the ground, and the bedload and part of the suspended load are deposited in the landslide-dammed lake (Morche and Schmidt, 2012). However, in case of partial dam failure or dam overspilling, the water runs over the remnant landform and the fluvial sediments are not retained as efficiently: only a fraction of the upstream eroded sediments deposits in the landslide-dammed lake. Furthermore, the drop in lake level induces the incision of the previous delta surface, and sediments deposit closer to the dam and in the incised delta, as an inset delta sequence (Winsemann et al., 2011). Thus, a dam that fully impounded the river flow but underwent a partial failure would be associated with a decreasing sediment infilling rate in the upstream lake and an incised delta topography in the upstream part of the valley, a landform that we did not observe.

6.5. Rheology, landslide types and dam longevity potential

Landslides are usually classified into different types (Varnes, 1978) based on the landsliding process and the type of material involved. Since the composition of landslides (e.g., clay and water content) affects their rheology (see Section 6.2), landslide rheology is therefore related to landslide type.

Most landslide dams (> 80%) fail within the first year (Costa and Schuster, 1988), but at different rates depending on the landslide type (Fan et al., 2020). Indeed, in the long term (after 10 years), rock avalanche, debris flow, debris avalanche, and unconsolidated landslide dams have similar longevity. However, in the short term (within the first few hours/days), debris flow dams tend to fail more quickly than rock avalanche dams (such as the Hintersee).

The stability of landslide dams is also controlled by the degree of debris fracturing (Weidinger, 2011) and the internal structure of the dam (Fan et al., 2017). Overall, the longer the landslide travels, the stronger the debris fracturing, and the less robust the dam forms (Weidinger, 2011). The internal structure of dams, meanwhile, can be classified into three types (Fan et al., 2017): long-runout slides, composed of unconsolidated debris, with low stability and high erodibility (e.g., Donghekou and Xiejiadianzi landslides, Fan et al., 2017); dams consisting of large blocks forming a shell on top of more fragmented debris, which are more stable (e.g., Falling Mountain rock avalanche, Davies and McSaveney, 2002); and dams formed from an intact stratum of bedrock at the base covered by debris, the most stable of all (e.g., Xiaojiaqiao dam Fan et al., 2017). In the case of the Hintersee dam, the short runout distance and large boulders scattered over the study area point to low fracturing and a structure with shell, thus relatively stable.

7. Conclusions

In this study, we investigate the impact of landslide rheology on the formation of landslide dams and their associated lacustrine deltas by back-analyzing the Hintersee landslide dam. We first reconstruct the pre-landslide topography based on literature and geophysical data, then simulate several landsliding scenarios with different release volumes and landslide rheologies, and finally compute the resulting dammed-lake and lacustrine delta topographies. We obtain the best reproduction of the current topography with a Voellmy rheology of $\mu = 0.08$ and $\xi = 300$ m.s^{-2}. Furthermore, we find that:

1. There is an important subaerial component to the sediment trapping capacity of landslide dams: here, the volume of trapped sediment exceeds the volume of the landslide-dammed lake by a factor of three.
2. Different landslide styles and valley geometries (accomodation spaces) create different types of dams, associated lakes and sediment trap capacities. Specifically, landslide rheology exhibits a non-linear relationship with lake volume and sediment trap capacity. The optimal rheology for the greatest sediment trap capacity is determined by valley topography.
3. Dry friction μ has more control over landslide-dammed lake formation and volume than velocity squared drag ξ.
4. By comparing our results to previous studies, we find that rock avalanches on unsaturated or bedrock substrates could be less likely to dam large lakes and form sediment traps.
5. Our findings suggest that the Hintersee landslide dam may have never breached catastrophically.
6. Based on trapped sediment volumes and age of the landslide, erosion rates in the valley could reach 230 mm.ka^{-1}.
7. By analyzing the dam morphology, we find that the dam was eroded with an average rate of 850 mm.ka^{-1} and a maximum rate of 7930 mm.ka^{-1}.

Code availability statement

The runout code is available online from Argentin et al. (2021), and has been encapsulated in a Docker container for easy setup: DOI: https://doi.org/10.5281/zenodo.4171597.

CRediT authorship contribution statement

Anne-Laure Argentin: Conceptualization, Methodology, Validation, Formal analysis, Investigation, Data curation, Writing – original draft, Writing – review & editing, Visualization, Supervision. **Thomas Hauthaler:** Methodology, Validation, Formal analysis, Investigation, Writing – original draft, Writing – review & editing, Visualization. **Moritz Liebl:** Writing – review & editing. **Jörg Robl:** Conceptualization, Methodology, Writing – review & editing, Supervision. **Stefan Hergarten:** Writing – review & editing. **Günther Prasicek:** Funding acquisition, Writing – review & editing, Supervision, Project administration. **Bernhard Salcher:** Writing – review & editing. **Daniel Hölbling:** Funding acquisition, Data curation, Writing – review & editing, Project administration. **Claire Pfalzner-Gibbon:** Data curation, Writing – review & editing. **Lisa Mandl:** Data curation, Writing – review & editing. **Michael Maroschek:** Data curation, Writing – review & editing. **Lorena Abad:** Writing – review & editing. **Zahra Dabiri:** Writing – review & editing.

Declaration of competing interest

The authors declare that they have no conflict of interest.

Acknowledgments

Schlumberger® is acknowledged for providing the software Petrel® for 3D modeling. The authors thank the Berchtesgaden National Park for providing the DEM and complementary documentation. This research has been supported by the Austrian Academy of Sciences (ÖAW) through the project RiCoLa (Detection and analysis of landslide-induced river course changes and lake formation). A.-L.A. was supported by a Marie Andeßner grant. We also thank the two anonymous reviewers and the editor for their constructive comments.

Appendix A

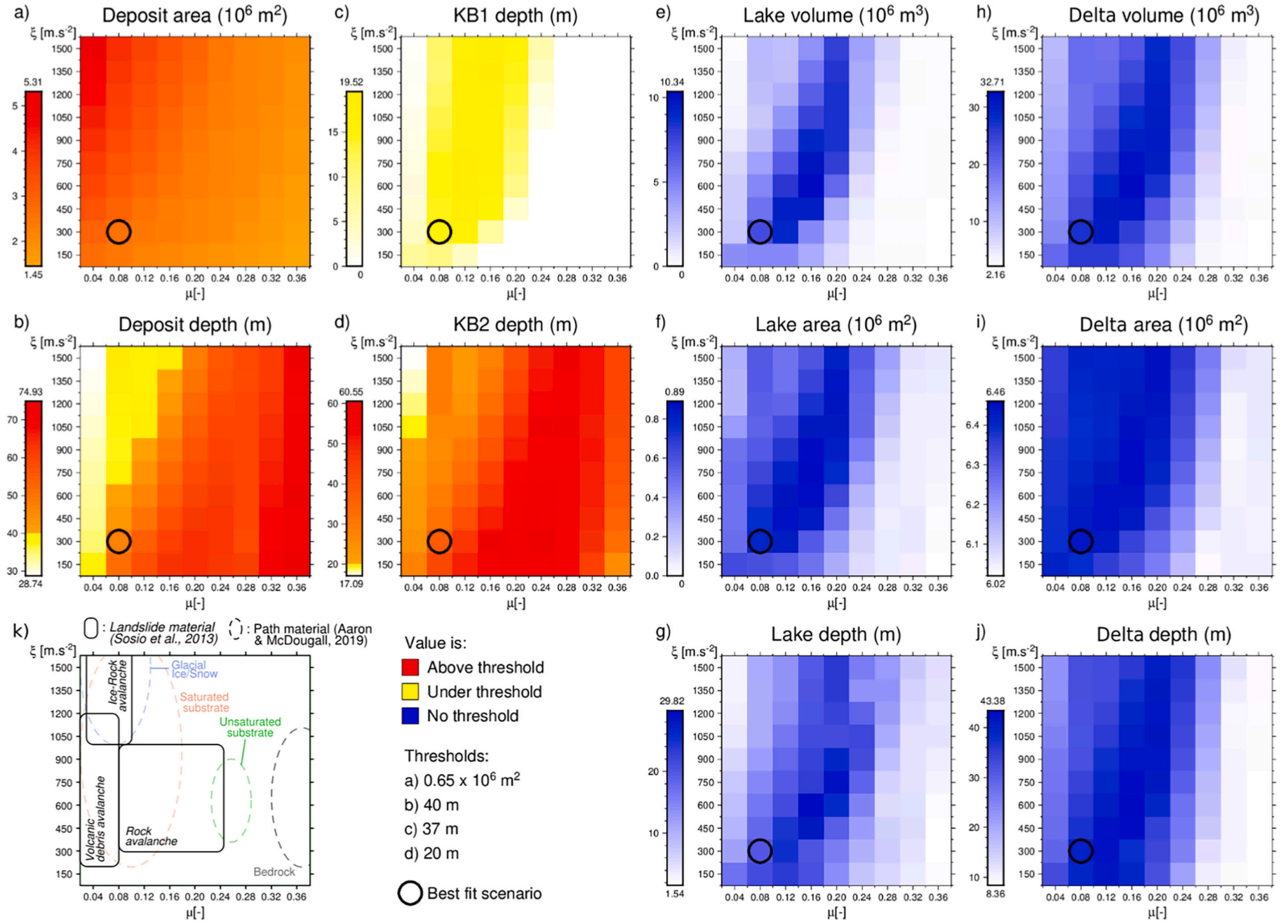

Fig. B.12. Influence of the Voellmy parameters - the dry friction μ and the velocity squared drag ξ - on the geometries of the landslide dam (a-d), landslide-dammed lake (e-g), and lacustrine delta (h-j) for source area 1. Values are plotted using a color gradient and compared to indicative thresholds when available: a) the area and b) depth of landslide deposit predicted by von Poschinger and Thom (1995), c) the minimum landslide deposit depth found in borehole KB1 and d) KB2 by Risch (1993). Values above the thresholds are plotted in red, those below in yellow, and those without indication in blue. The best fit scenario found based on the plan and cross-section geometries is highlighted by a circle.

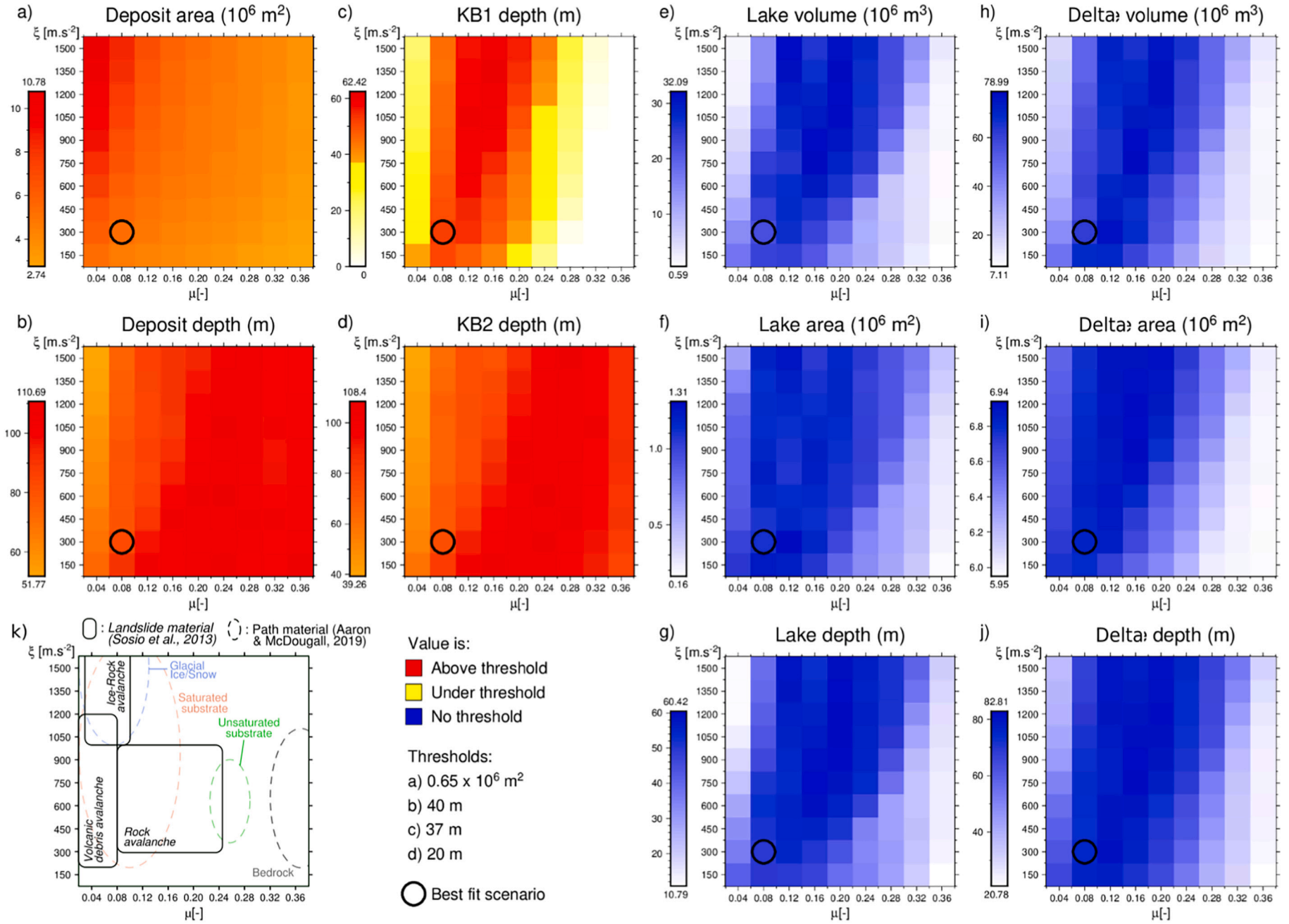

Fig. B.13. Influence of the Voellmy parameters - the dry friction μ and the velocity squared drag ξ - on the geometries of the landslide dam (a-d), landslide-dammed lake (e-g), and lacustrine delta (h-j) for source area 3. Values are plotted using a color gradient and compared to indicative thresholds when available: a) the area and b) depth of landslide deposit predicted by von Poschinger and Thom (1995), c) the minimum landslide deposit depth found in borehole KB1 and d) KB2 by Risch (1993). Values above the thresholds are plotted in red, those below in yellow, and those without indication in blue. The best fit scenario found based on the plan and cross-section geometries is highlighted by a circle.

Appendix B. Supplementary data

Supplementary data to this article can be found online at https://doi.org/10.1016/j.geomorph.2022.108363.

References

Aaron, J., McDougall, S., 2019. Rock avalanche mobility: the role of path material. Eng. Geol. 257 https://doi.org/10.1016/j.enggeo.2019.05.003.

Argentin, A.-L., Robl, J., Prasicek, G., Hergarten, S., Hölbling, D., Abad, L., Dabiri, Z., 2021. Controls on the formation and size of potential landslide dams and dammed lakes in the Austrian Alps. Nat. Hazards Earth Syst. Sci. 21, 1615–1637. https://doi.org/10.5194/nhess-21-1615-2021.

Bader, K., 1981. Die glazialen Ubertiefungen im Saalachgletscher-Gebiet zwischen Inzell und Konigssee. Eiszeit. Gegenw. 31, 37–52. https://doi.org/10.3285/eg.31.1.04.

Bayerisches Geologisches Landesamt, 2005. URL: https://www.lfu.bayern.de/geologie/bayerns_schoenste_geotope/46/doc/46_schautafel.pdf.

Bayerisches Landesamt für Umwelt, 1993. Geologische karte 1:25.000 - 8343 berchtesgaden west, datenquelle: Bayerisches landesamtfür umwelt. www.lfu.bayern.de.

Blair, T.C., McPherson, J.G., 1994. Alluvial fans and their natural distinction from rivers based on morphology, hydraulic processes, sedimentary processes, and facies assemblages. J. Sedimentary Res. A 450–489. https://doi.org/10.1306/d42681b7-2b26-11d7-8648000102c1865d.

Blöthe, J.H., Korup, O., 2013. Millennial lag times in the Himalayan sediment routing system. Earth Planet. Sci. Lett. 382, 38–46. https://doi.org/10.1016/j.epsl.2013.08.044.

Bond, C.E., 2015. Uncertainty in structural interpretation: lessons to be learnt. J. Struct. Geol. 74, 185–200. https://doi.org/10.1016/j.jsg.2015.03.003.

Christen, M., Kowalski, J., Bartelt, P., 2010. RAMMS: numerical simulation of dense snow avalanches in three-dimensional terrain. Cold Reg. Sci. Technol. 63, 1–14. https://doi.org/10.1016/j.coldregions.2010.04.005.

Codilean, A.T., Munack, H., Cohen, T.J., Saktura, W.M., Gray, A., Mudd, S.M., 2018. OCTOPUS: an open cosmogenic isotope and luminescence database. Earth Syst. Sci. Data 10, 2123–2139. https://doi.org/10.5194/essd-10-2123-2018.

Cossart, E., Fort, M., 2008. Consequences of landslide dams on alpine river valleys: examples and typology from the French Southern Alps. Nor. Geol. Tidsskr. 62, 75–88. https://doi.org/10.1080/00291950802094882.

Costa, J.E., Schuster, R.L., 1988. Formation and failure of Natural Dams. Bull. Geol. Soc. Am. 100, 1054–1068. https://doi.org/10.1130/0016-7606(1988)100<1054:TFAFON>2.3.CO.

Crosta, G.B., Frattini, P., 2004. Controls on modern alluvial fan processes in the Central Alps, Northern Italy. Earth Surf. Process. Landf. 29, 267–293. https://doi.org/10.1002/esp.1009.

Dade, W.B., Friend, P.F., 1998. Grain-Size, Sediment-Transport Regime, and Channel Slope in Alluvial Rivers 1, Technical Report.

Davies, T.R., McSaveney, M.J., 2002. Dynamic simulation of the motion of fragmenting rock avalanches. Can. Geotech. J. 39, 789–798. https://doi.org/10.1139/t02-035.

Delaney, K.B., Evans, S.G., 2015. The 2000 Yigong landslide (Tibetan Plateau), rockslide-dammed lake and outburst flood: review, remote sensing analysis, and process modelling. Geomorphology 246, 377–393. https://doi.org/10.1016/j.geomorph.2015.06.020.

Delunel, R., Schlunegger, F., Valla, P.G., Dixon, J., Glotzbach, C., Hippe, K., Kober, F., Molliex, S., Norton, K.P., Salcher, B., Wittmann, H., Akçar, N., Christl, M., 2020. Late-Pleistocene Catchment-wide Denudation Patterns Across the European Alps. https://doi.org/10.1016/j.earscirev.2020.103407.

Fan, X., van Westen, C.J., Korup, O., Gorum, T., Xu, Q., Dai, F., Huang, R., Wang, G., 2012. Transient water and sediment storage of the decaying landslide dams induced by the 2008 Wenchuan earthquake, China. Geomorphology 171-172, 58–68. https://doi.org/10.1016/j.geomorph.2012.05.003.

Fan, X., Xu, Q., van Westen, C.J., Huang, R., Tang, R., 2017. Characteristics and classification of landslide dams associated with the 2008 Wenchuan earthquake. Geoenviron. Disasters 4. https://doi.org/10.1186/s40677-017-0079-8.

Fan, X., Dufresne, A., Subramanian, S.Siva, Strom, A., Hermanns, R., Stefanelli, C. Tacconi, Hewitt, K., Yunus, A.P., Dunning, S., Capra, L., Geertsema, M., Miller, B., Casagli, N., Jansen, J.D., Xu, Q., 2020. The Formation and Impact of Landslide Dams – State of the Art. https://doi.org/10.1016/j.earscirev.2020.103116.

Glotzbach, C., Van Der Beek, P., Carcaillet, J., Delunel, R., 2013. Deciphering the driving forces of erosion rates on millennial to million-year timescales in glacially impacted landscapes: an example from the Western Alps. J. Geophys. Res. Earth Surf. 118, 1491–1515. https://doi.org/10.1002/jgrf.20107.

Grischott, R., Kober, F., Lupker, M., Hippe, K., Ivy-Ochs, S., Hajdas, I., Salcher, B., Christl, M., 2017. Constant denudation rates in a high alpine catchment for the last 6 kyrs. Earth Surf. Process. Landf. 42, 1065–1077. https://doi.org/10.1002/esp.4070.

Hack, J.T., 1957. Studies of Longitudinal Stream Profiles in Virginia and Maryland, US Geol. Survey Prof. Papers, 294-B. US Government Printing Office, Washington D.C., USA.

Hergarten, S., Robl, J., 2015. Modelling rapid mass movements using the shallow water equations in Cartesian coordinates. Nat. Hazards Earth Syst. Sci. 15, 671–685. https://doi.org/10.5194/nhess-15-671-2015.

Hinderer, M., 2001. Late quaternary denudation of the alps, valley and lake fillings and modern river loads. Geodin. Acta 14, 231–263. https://doi.org/10.1080/09853111.2001.11432446.

Hinderer, M., 2012. From Gullies to Mountain Belts: A Review of Sediment Budgets at Various Scales. https://doi.org/10.1016/j.sedgeo.2012.03.009.

Hungr, O., 2011. Prospects for prediction of landslide dam geometry using empirical and dynamic models. In: Natural and Artificial Rockslide Dams. Springer, pp. 463–477.

Hungr, O., Evans, S., 1996. Rock avalanche runout prediction using a dynamic model. URL: http://www.clara-w.com/DANWReference2.pdf.

Hungr, O., Evans, S.G., 2004. Entrainment of debris in rock avalanches: an analysis of a long run-out mechanism. Bull. Geol. Soc. Am. 116, 1240–1252. https://doi.org/10.1130/B25362.1.

Hürlimann, M., McArdell, B.W., Rickli, C., 2015. Field and laboratory analysis of the runout characteristics of hillslope debris flows in switzerland. Geomorphology 232, 20–32. https://doi.org/10.1016/j.geomorph.2014.11.030.

Hussin, H.Y., Luna, B.Quan, Westen, C.J.Van, Christen, M., Malet, J.P., Asch, T.W.Van, 2012. Parameterization of a numerical 2-D debris flow model with entrainment: a case study of the Faucon catchment, Southern French Alps. Nat. Hazards Earth Syst. Sci. 12, 3075–3090. https://doi.org/10.5194/nhess-12-3075-2012.

Ilyashuk, E.A., Koinig, K.A., Heiri, O., Ilyashuk, B.P., Psenner, R., 2011. Holocene temperature variations at a high-altitude site in the Eastern Alps: a chironomid record from Schwarzsee Ob Sölden, Austria. Quat. Sci. Rev. 30, 176–191. https://doi.org/10.1016/j.quascirev.2010.10.008.

Korup, O., 2005. Geomorphic hazard assessment of landslide dams in South Westland, New Zealand: fundamental problems and approaches. Geomorphology 66, 167–188. https://doi.org/10.1016/j.geomorph.2004.09.013.

Korup, O., Schlunegger, F., 2009. Rock-type control on erosion-induced uplift, eastern Swiss Alps. Earth Planet. Sci. Lett. 278, 278–285. https://doi.org/10.1016/j.epsl.2008.12.012.

Landesamt für Digitalisierung, 2017. Breitband und Vermessung, Digital elevation model of ramsau berchtesgaden.

Lin, C.H., Lin, M.L., 2015. Evolution of the large landslide induced by Typhoon Morakot: a case study in the Butangbunasi River, southern Taiwan using the discrete element method. Eng. Geol. 197, 172–187. https://doi.org/10.1016/j.enggeo.2015.08.022.

Morche, D., Schmidt, K.H., 2012. Sediment transport in an alpine river before and after a dambreak flood event. Earth Surf. Process. Landf. 37, 347–353. https://doi.org/10.1002/esp.2263.

Naaim, M., Durand, Y., Eckert, N., Chambon, G., 2013. Dense avalanche friction coefficients: influence of physical properties of snow. J. Glaciol. 59, 771–782. https://doi.org/10.3189/2013JoG12J205.

Ouimet, W.B., Whipple, K.X., Royden, L.H., Sun, Z., Chen, Z., 2007. The influence of large landslides on river incision in a transient landscape: Eastern margin of the Tibetan Plateau (Sichuan, China). Bull. Geol. Soc. Am. 119, 1462–1476. https://doi.org/10.1130/B26136.1.

Penck, A., Richter, E., 1885. In: Das Land Berchtesgaden, Zeitschr. d. Dt. u. Österr. Alpenvereins, 16, pp. 217–298. https://anno.onb.ac.at/cgi-content/anno-plus?aid=oav&datum=1885&page=227&size=46.

Pomper, J., Salcher, B.C., Eichkitz, C., Prasicek, G., Lang, A., Lindner, M., Götz, J., 2017. The glacially overdeepened trough of the Salzach Valley, Austria: bedrock geometry and sedimentary fill of a major Alpine subglacial basin. Geomorphology 295, 147–158. https://doi.org/10.1016/j.geomorph.2017.07.009.

Popinet, S., 2003. Gerris: a tree-based adaptive solver for the incompressible Euler equations in complex geometries. J. Comput. Phys. 190, 572–600. https://doi.org/10.1016/S0021-9991(03)00298-5.

von Poschinger, A., Thom, P., 1995. Bergsturz Hintersee/Ramsau (Berchtesgadener Land): Neue Untersuchungsergebnisse. Geologica Bavarica 99, 399–411.

Pratt-Sitaula, B., Garde, M., Burbank, D.W., Oskin, M., Heimsath, A., Gabet, E., 2007. Bedload-to-suspended load ratio and rapid bedrock incision from Himalayan landslide-dam lake record. Quat. Res. 68, 111–120. https://doi.org/10.1016/j.yqres.2007.03.005.

Risch, H., 1993. Geologische Karte von Bayern 1:25 000, Erläuterungen zum Blatt Nr. 8343 Berchtesgaden West, Technical Report. Bayerisches Geologisches Landesamt, München.

Savage, S.B., Hutter, K., 1989. The motion of a finite mass of granular material down a rough incline. J. Fluid Mech. 199, 177–215. https://doi.org/10.1017/S0022112089000340.

Savelli, D., Troiani, F., Brugiapaglia, E., Calderoni, G., Cavitolo, P., Dignani, A., Ortu, E., Teodori, S., Veneri, F., Nesci, O., 2013. The landslide-dammed paleolake of Montelago (North-Marche Apennines, Italy): geomorphological evolution and paleoenvironmental outlines. Geogr. Fis. Din. Quat. 36, 267–287. https://doi.org/10.4461/GFDQ.2013.36.22.

Schlumberger, 2010. Petrel Help Manual. Schlumberger, Houston.

Schraml, K., Thomschitz, B., Mcardell, B.W., Graf, C., Kaitna, R., 2015. Modeling debris-flow runout patterns on two alpine fans with different dynamic simulation models. Nat. Hazards Earth Syst. Sci. 15, 1483–1492. https://doi.org/10.5194/nhess-15-1483-2015.

Schwanghart, W., Scherler, D., 2014. Short communication: TopoToolbox 2 - MATLAB-based software for topographic analysis and modeling in Earth surface sciences. Earth Surf. Dyn. 2, 1–7. https://doi.org/10.5194/esurf-2-1-2014.

Scott, K.M., Macías, J.L., Naranjo, J.A., Rodríguez, S., McGeehin, J.P., 2001. Catastrophic debris flows transformed from landslides in volcanic terrains: mobility, hazard assessment, and mitigation strategies. In: US Geological Survey Professional Paper, pp. 1–59.

Shen, W., Li, T., Li, P., Shen, Y., Lei, Y., Guo, J., 2019. The influence of the bed entrainment-induced rheology and topography changes on the propagation of flow-like landslides: a numerical investigation. Bull. Eng. Geol. Environ. 78, 4771–4785. https://doi.org/10.1007/s10064-018-01447-1.

Sosio, R., Crosta, G.B., Chen, J.H., Hungr, O., 2013. Runout prediction of rock avalanches in volcanic and glacial terrains. In: Margottini, C., Canuti, P., Sassa, K. (Eds.),

Landslide Science and Practice: Spatial Analysis and Modelling, volume 3. Springer Berlin, Heidelberg, pp. 285–291. https://doi.org/10.1007/978-3-642-31310-3_38.
Stolle, A., Schwanghart, W., Andermann, C., Bernhardt, A., Fort, M., Jansen, J.D., Wittmann, H., Merchel, S., Rugel, G., Adhikari, B.R., Korup, O., 2019. Protracted river response to medieval earthquakes. Earth Surf. Process. Landf. 44, 331–341. https://doi.org/10.1002/esp.4517.
Varnes, D.J., 1978. In: Slope Movement Types and Processes, Transportation Research Board Special Report, pp. 11–33.
Voellmy, A., 1955. In: Über die Zerstörungskraft von Lawinen, 73. Schweizerische Bauzeitung, pp. 159–165. https://doi.org/10.5169/seals-61891.
Wang, L., Liu, H., 2006. An efficient method for identifying and filling surface depressions in digital elevation models for hydrologic analysis and modelling. Int. J. Geogr. Inf. Sci. 20, 193–213. https://doi.org/10.1080/13658810500433453.
Wang, P., Scherler, D., Liu-Zeng, J., Mey, J., Avouac, J.P., Zhang, Y., Shi, D., 2014. Tectonic control of Yarlung Tsangpo Gorge revealed by a buried canyon in Southern Tibet. Science 346, 978–981. https://doi.org/10.1126/science.1259041.
Weidinger, J., 2011. URL:. In: Stability and Life Span of Landslide Dams in the Himalayas (India, Nepal) and the Qin Ling Mountains (China). Springer, Berlin Heidelberg, Berlin, Heidelberg, pp. 243–277 https://doi.org/10.1007/978-3-642-04764-0_8.
Wessel, P., Luis, J.F., Uieda, L., Scharroo, R., Wobbe, F., Smith, W.H., Tian, D., 2019. The generic mapping tools version 6. Geochem. Geophys. Geosyst. 20, 5556–5564. https://doi.org/10.1029/2019GC008515.
Winsemann, J., Brandes, C., Polom, U., 2011. Response of a proglacial delta to rapid high-amplitude lake-level change: an integration of outcrop data and high-resolution shear wave seismics. Basin Res. 23, 22–52. https://doi.org/10.1111/j.1365-2117.2010.00465.x.
Zimmermann, F., McArdell, B.W., Rickli, C., Scheidl, C., 2020. 2D runout modelling of hillslope debris flows, based on well-documented events in Switzerland. Geosciences (Switzerland) 10. https://doi.org/10.3390/geosciences10020070.